JACS
JOURNAL OF THE AMERICAN CHEMICAL SOCIETY
pubs.acs.org/JACS
Perspective

What Lies beneath a Metal−Organic Framework Crystal Structure? New Design Principles from Unexpected Behaviors

Mark D. Allendorf,* Vitalie Stavila, Matthew Witman, Carl K. Brozek, and Christopher H. Hendon

Cite This: https://doi.org/10.1021/jacs.0c10777
Read Online
ACCESS | Metrics & More | Article Recommendations

ABSTRACT: The rational design principles established for metal−organic frameworks (MOFs) allow clear structure−property relationships, fueling expansive growth for energy storage and conversion, catalysis, and beyond. However, these design principles are based on the assumption of compositional and structural rigidity, as measured crystallographically. Such idealization of MOF structures overlooks subtle chemical aspects that can lead to departures from structure-based chemical intuition. In this Perspective, we identify unexpected behavior of MOFs through literature examples. Based on this analysis, we conclude that departures from ideality are not uncommon. Whereas linker topology and metal coordination geometry are useful starting points for understanding MOF properties, we anticipate that deviations from the idealized crystal representation will be necessary to explain important and unexpected behaviors. Although this realization reinforces the notion that MOFs are highly complex materials, it should also stimulate a broader reexamination of the literature to identify corollaries to existing design rules and reveal new structure−property relationships.

1. INTRODUCTION

Metal−organic frameworks (MOFs) have captured the imagination and inspired the creativity of countless scientists because they are generally thought to adhere to a series of rational design principles that allow structures with specific properties to be designed and synthesized.[1] The appeal of MOFs stems in part from what appear to be rigid structures well-described by crystallography. One powerful consequence is that isoreticular series can be created, i.e., frameworks sharing the same geometric topology and connectivity, but with different linkers and/or metal ions.[2] In principle this modularity simplifies the design process and enables systematic investigation to uncover structure−property relationships. Consequently, the picture of MOFs as invariant, essentially rigid structures has been enormously successful for understanding many of their properties over the past 20 years.

The archetypal MOF image is often presented as an idealized, high-symmetry crystal with well-defined pores (Figure 1). However, the refined structures obtained from crystallography have limitations due to large void spaces that often feature poorly resolved guest molecules within the pores, as well as other familiar crystallographic challenges such as disorder and crystal twinning.[3] As a result, subtleties can sometimes be overlooked. We ourselves only recently appreciated the different pore environments and derivative chemistry of MOF-5, for example (Figure 2A).[4,5] In addition to challenges in pristine structure determination, all MOFs likely contain intrinsic defects in low concentrations and/or possess structural flexibility and dynamics that may evade standard X-ray techniques.

Hidden in the cavities of pores and at the microscopic interfaces between the metal ions and organic linkers lies chemical complexity that explains some of the most important MOF properties. For instance, subtle differences in the electrostatics of pore surfaces can explain large differences in gas uptake selectivity.[6,7] Large structural perturbations were recognized early on (e.g., "breathing" phase changes).[8−11] Later, vacancy defects were characterized, adding further complexity to these materials.[12] Finally, both disordered and amorphous

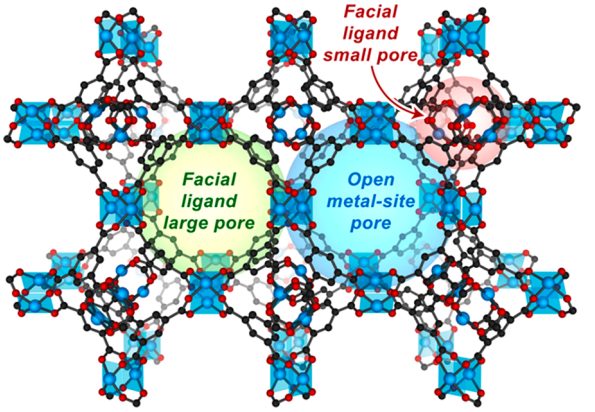

Figure 1. Pore structure of the archetypal MOF, $Cu_3(btc)_2$ (or HKUST-1), showing three distinct pore topologies. Facial is relative to the π-face of the ligand. C, O, and Cu atoms are shown in black, red, and blue, respectively. Reproduced with permission from ref 34. Copyright 2014 American Chemical Society.

Received: October 12, 2020

MOFs have been reported,[13−15] reaching beyond the ideal crystallographic picture (e.g., $Cu_3(btc)_2$ shown in Figure 1). In many such cases, the local chemical connectivity is maintained, while long-range order is disrupted.[16]

In this Perspective, we discuss a diverse collection of literature describing the tendency of MOFs to deviate from the behavior expected from their crystallographic representation. Our intent is not to provide a comprehensive review but rather to highlight the prevalence of these effects. In section 2 we give definitions to frame the discussion. Sections 3−6 discuss examples from most of the major MOF application fields, including gas storage,[17−21] separations,[20,22−24] catalysis and reactivity,[25] and conducting,[26,27] stimuli-responsive,[28] and luminescent[29−33] frameworks. We conclude that (1) even very subtle departures from crystallographic ideality can have strikingly large implications for MOF properties and (2) the prevalence of these effects extends far beyond more well-studied phenomena such as nonporous-to-porous phase changes or defects. Finally, in section 7, we summarize key opportunities stimulated by our expanded awareness of these intriguing MOF features.

2. CONCEPTS AND DEFINITIONS

In the most general sense, we use "misbehavior" and "incongruity" to refer to properties and phenomena exhibited by MOFs that do not conform to expectations based purely on a crystal structure or by extrapolating an invariant topology (e.g., within an isoreticular series). In this section we describe three basic assumptions (shown schematically in Figure 2) that lead to unexpected phenomena or properties: (1) crystallographic/structural misbehaviors resulting from an assumption of a static structure (i.e., the "idealized, rigid structure" assumption). These include both crystallographic polymorphism and amorphism (Figure 2B). (2) Local bonding misbehaviors at the metal−ligand interface, arising from the assumption that the structure is invariant regardless of whether the pores are empty or filled with solvent molecules (i.e., the "solvent-independence" assumption, Figure 2C). (3) Composition and oxidation state incongruities relative to expectations for a largely unreactive structure (i.e., the "static electronic structure" assumption, Figure 2D). These can arise when transmetalation or ligand substitution leads to a redox-active metal, ligand, or both.

2.1. Structural and Crystallographic Misbehaviors.

There is often more than meets the eye when considering a crystal structure. From an experimental viewpoint, crystal structures are typically obtained at cryogenic temperatures, which reduce phonons' contributions to the electronic structure. We tend to favor high-symmetry crystal settings, even if it increases disorder of functional groups and/or guests within the pores. However, even within these approximations, subtle differences are still revealed, most fundamentally demonstrated by differences between neighboring pores. For example, the archetypal MOF UiO-66, Figure 3, features a Freundlich type I gas sorption isotherm when measured with a non-polar guest (we present CH_4, but a similar isotherm is observed with essentially all non-polar probe molecules) but a Sigmoid-type V isotherm when probed with water.[35] Although one proposed explanation is that this difference is due to dehydroxylation of the MOF node (which itself is a misbehavior),[36] another is that the capillary condensation of water in the small pore is not captured with non-interacting gases. This example hence demonstrates that even within one of the most well-studied MOFs to date, there exist subtleties that may be overlooked by conventional characterization methods.

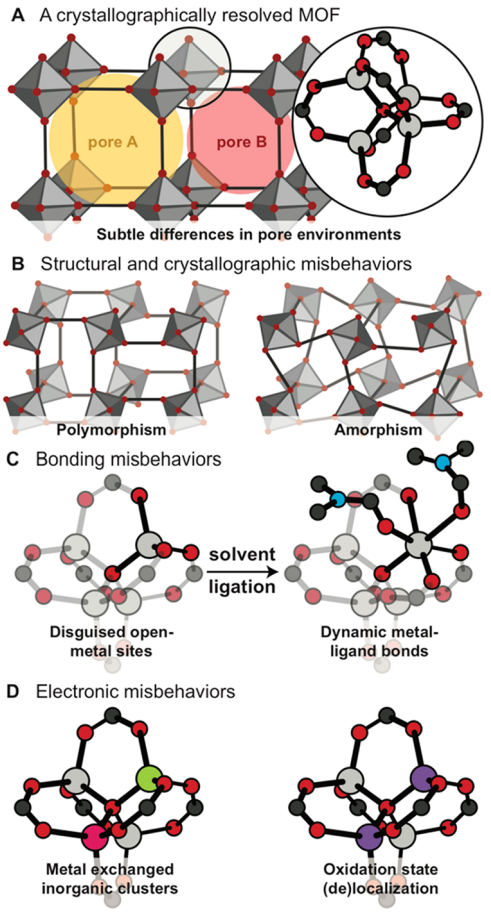

Figure 2. (A) Pristine MOF depictions can occlude three categories of misbehaviors, based on the assumptions that (B) MOF structures are rigid, (C) the transition metal inner coordination sphere is static, and (D) the electronic structure is static.

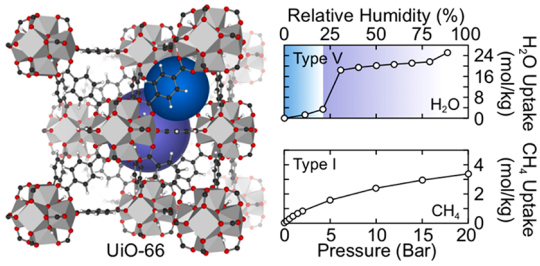

Figure 3. The archetypal MOF, UiO-66, features two distinct pores revealed upon filling with water. The same Type V feature is not seen when the pores are filled with methane, because of the reduced surface tension of methane.

2.1.1. Pore Structure. Beyond the examples of UiO-66 and MOF-5, many other MOFs feature subtle differences in similarly sized pores. For example, the pores of $Cu_3(btc)_2$, which shares the same $Fm\bar{3}m$ symmetry as MOF-5, feature a more dramatic departure from a first impression of the structure. The original report[37] states that this MOF has "1-nm channels with four-fold symmetry", leading to a 3D porous network. The well-known Cu(II) open metal sites (OMSs) within the framework are described as being "directed from the copper atoms to the interior of the nanopores". One infers from this that $Cu_3(btc)_2$ consists of a cubic lattice of identical pores. On the contrary, careful inspection of the crystal structure shows that this MOF

https://doi.org/10.1021/jacs.0c10777
J. Am. Chem. Soc. XXXX, XXX, XXX−XXX

has *three* distinct pore types (pore sizes computed using the Zeo ++ code[38]): one large pore (~1.3 nm) with 12 unsaturated Cu-ions pointing into the pore volume; a second somewhat smaller pore (~1.1 nm) with the axis of the copper paddlewheels pointing tangential to the pore volume; and a third, much smaller pore (~0.55 nm) with no OMSs (see Figure 1).[39,40] This is important, because we often invoke the high-density of OMSs in MOFs as an argument for their use in catalysis, whereas in reality not all pores may feature OMS active sites.

2.1.2. Hindered Linker Internal Rotation and Distortion. The coaxial rings of some polyphenyl linkers (e.g., linkers used in the NOTT series;[41,42] bold lines in Figure 4a) can rotate about

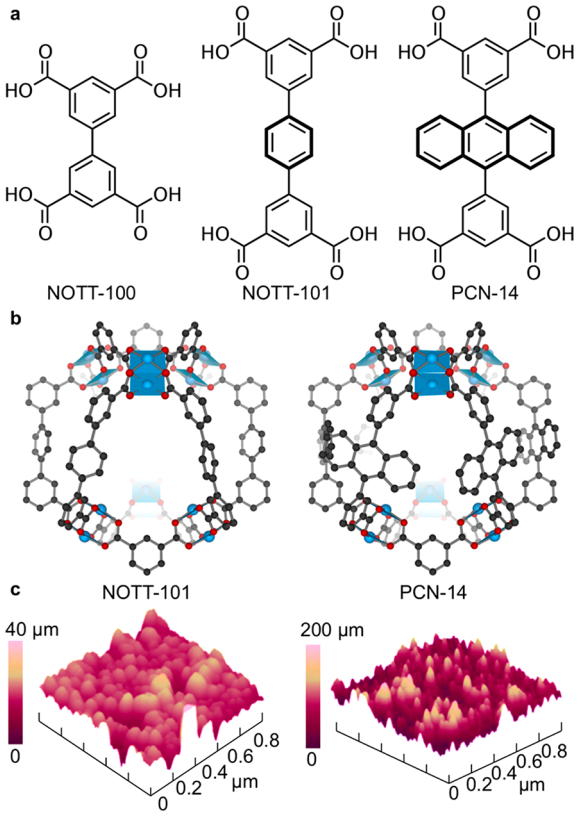

Figure 4. (a) The linkers used to form the majority of the NOTT series are isostructural with the linker in PCN-14. Rings in bold can rotate. (b) Both NOTT-101 and PCN-14 are isostructural, but only the former features room-temperature ring rotation. (c) Macroscopically, the structures made with the less sterically hindered ligand tend to form smoother films, attributed to slow adhesion of the anthracene-containing linker forming bonds with the substrate. Reprinted in part with permission from ref 45. Copyright 2016 John Wiley and Sons.

the linker axis. Linker sterics can be used to prevent ring rotation, as in PCN-14.[43] The true misbehavior, however, manifests in the impact of hindered linker rotation upon the morphology of thin films of these MOFs: a microscopic chemical interaction that dictates the macroscopic morphological properties of the material. This has been demonstrated by depositing several NOTT MOFs using layer-by-layer methods,[44] including NOTT-100, NOTT-101,[45] and $Cu_3(btc)_2$[46] (example structures are shown in Figure 4b). Films of these on oxide substrates are oriented, dense, and very smooth, with root-mean-squared roughness ~6−20 nm (Figure 4c). In contrast, layer-by-layer growth of PCN-14 is too slow, instead requiring a high-temperature solvothermal approach. The resulting films are polycrystalline with random orientation and a morphology similar to that of Styrofoam but with a much higher roughness than the other two MOFs. Thus, while the MOFs themselves may have similar properties, the synthetic considerations dramatically alter the bulk properties of the materials.

2.1.3. Disorder in MOFs. *Structural disorder* in MOFs arises primarily during synthesis, where many similar energy configurations compete. Beyond thermodynamic wells, kinetic traps may exist. Additionally, solvent and guest molecules in the pores contribute to the overall Bragg diffraction, but can cause loss ("washing-out") of high-resolution reflections at 2θ.[3,51−53] Other contributing factors include poorly diffracting single crystals and localized disorder or amorphous phases.[51] Reactant mixtures of organic linkers,[47,48] metal ions,[49,50] and secondary building units (SBUs)[51,52] also can lead to disorder, posing significant challenges for structure solution and determining accurate atomic positions. Post-synthetic modification (PSM) and solvent-assisted linker exchange (SALE) used to functionalize MOFs[54,55] are other sources of disorder,[56,57] due to incomplete ligand or metal exchange.[58,59] Finally, single crystals are often not available, requiring structure determinations using powder data[60,61] and first-principles calculations.[62,63]

For MOFs without disorder, structure determination is straightforward. However, if disordered groups are present, identifying a realistic crystallographic model can be challenging.[3,52,64] Probability ellipsoids can give a general idea of the atomic positions and often these can provide information concerning crystal quality and data collection.[3] For example, the originally reported MOF-5 structure determination included data for two crystals, one fully solvated that gave a structure solution with an R-factor of 11%, the other desolvated that gave an R-factor of 2.3%.[53]

Typically, atomic motion is described by harmonic oscillation around the coordinates attributed to an atom. In this "independent atom model",[54] electrons are assumed to be spherically distributed, and the only deformations are those caused by thermal motion. Whereas the atomic oscillations nominally have a circular path, the electron density of the vibrating atom has non-linear harmonic motion. In MOFs, this parameter is usually sensitive to temperature, and therefore such effects can be decreased by reducing the temperature for data collection. However, there are exceptions to this guideline; for example, Yaghi and co-workers recently reported high-quality crystal structures for MOF-1004 and MOF-1005 at 290 K.[55] Incongruously, the quality of the MOF-1004 diffraction data is higher at room temperature than at 100 K (Figure 5). MOF-177

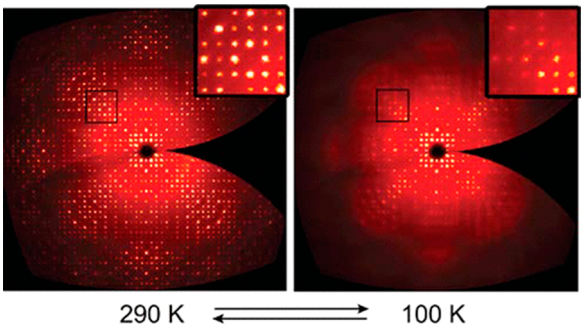

Figure 5. Room-temperature versus 100 K SCXRD in MOF-1004. Reproduced with permission from ref 55. Copyright 2018 American Chemical Society.

https://doi.org/10.1021/jacs.0c10777
J. Am. Chem. Soc. XXXX, XXX, XXX−XXX

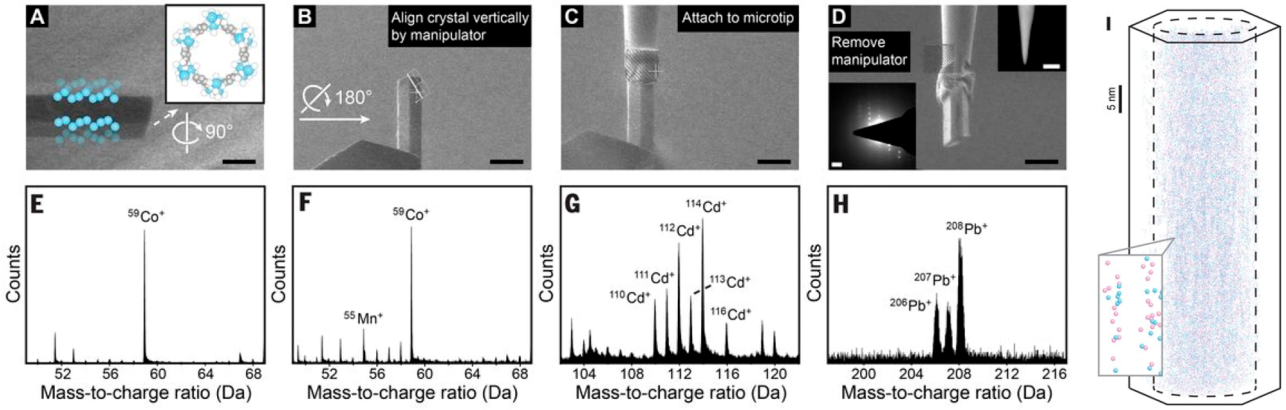

Figure 6. A single crystal of Co,Cd-MOF-74 (A) attached to a nanomanipulator, (B) aligned vertically, (C) welded to a Si microtip, (D) detached from the nanomanipulator, and (D, inset) sharpened into a tip shape. Selected-area electron diffraction patterns obtained from the APT tip are then indexed within the MOF-74 space group. Scale bars, 2 μm (bottom left inset of D, 2 nm). (E–H) The mass spectra of mixed-metal MOF-74 samples identified (E) $^{59}Co^+$, (F) $^{55}Mn^+$, (G) Cd^+, and (H) Pb^+ isotopes. (I) 3D atom probe tomography reconstruction shows 56 605 detected metal atoms from a single crystal of Co,Cd-MOF-74. Reprinted in part with permission from ref 60. Copyright 2020 The American Association for the Advancement of Science.

and UiO-67 also behave counterintuitively. Guest–framework interactions are ordered at room temperature but severely disordered at low temperature. Weaker guest–framework interactions at high temperatures reduce disorder, yielding high-resolution diffraction data sufficient for structure determination.[55]

Functional groups of similar size and binding properties can occupy equivalent places in a MOF structure, causing *substitutional disorder*. Accurate knowledge of MOF composition is extremely important to understand the partial occupancies and to refine such disorder. In practice, the bond lengths can vary upon substitution, resulting in a diffuse coordination environment and unreasonable displacement parameters.[56] The limitations of single-crystal X-ray diffraction (SCXRD) are particularly evident in multivariate MOFs, where multiple organic functionalities[57] and/or metal ions[58] are incorporated into a MOF backbone. Using SCXRD, the identity and ratio of the variate units can be quantified, but determining their spatial arrangement is extremely challenging.[59] Other spatially resolved probes must therefore be used. For example, 10 different divalent metals (Mg, Ca, Sr, Ba, Mn, Fe, Co, Ni, Zn, and Cd) can be used to form the MOF-74 topology and all 10 can be simultaneously incorporated within the structure.[58] Using energy-dispersive X-ray spectroscopy applied to crystalline powders, it was determined that the metal ion distribution is not uniform. More recently, Yaghi and co-workers determined the metal sequencing by atom probe tomography (APT) for MOF-74 single crystals containing combinations of cobalt, cadmium, lead, and manganese ions. They found that heterogeneities and sequences can either be random or have long- or short-range ordering, depending on the proportion of metals and synthesis conditions (Figure 6).[60]

In summary, structural disorder and heterogeneities are key features of MOFs. Although SCXRD continues to play a pivotal role in the development of MOFs, this class of materials has revealed important limitations of the technique, particularly over the past few years. For example, SCXRD often fails to describe MOF nanoparticles with various surface termination and complex disordered or semi-crystalline materials.[3,61,62] Other analytical techniques are being introduced to complement XRD and are showing tremendous promise, such as pair distribution function (PDF),[63] extended X-ray absorption fine structure (EXAFS),[64] APT,[60] and electron imaging[65] and diffraction.[66]

2.1.4. MOF Polymorphism. A cornerstone of targeted MOF synthesis is the predictable geometric connectivity enabled by a design paradigm based on minimal edge-transitive nets. This allows the entire chemical space to be readily described by combining all possible shapes and connections. However, a shortcoming of this approach is the potential for polymorphs that formally share the same transitive net but feature different terminal connectivity. In practice, examples of polymorphism are rare; whereas the number of reported crystal structures and compositions continues to increase, very few publications examine the phase space for a given composition. Nevertheless, multiple structures are routinely isolated from a given reaction mixture, but these typically have different stoichiometries. A true misbehavior is observed when materials with nominally the same stoichiometry feature either different chemical connectivity or diminished long-range order, i.e., metastable and non-equilibrium isomers that co-exist within a given compositional phase space. These polymorphs can be isolated from the same reaction mixture and can be targeted by both thermodynamic and kinetic crystal growth.[67,68]

In general, polymorphism is enabled by linker flexibility and dynamic metal-linker bonding. It is becoming increasingly common to observe linker distortions in molecules thought to be rigid.[69] Two recent studies embody these principles. Lee et al. recently demonstrated a single crystal-to-single crystal transition between kinetically isolated EHU-10 and thermodynamically preferable UiO-66.[70] This is a particularly compelling example because the linker is estimated to be 3 kcal/mol less stable in the former yet can be selectively synthesized under certain temperature regimes. In another study, Friščić and colleagues showed that phase transitions occur in zeolitic imidazolate frameworks (ZIFs);[71,72] these can even be pushed to complete amorphization.[73] Yet, there are no reports of polymorphism enabled by MOFs with identical stoichiometry but dissimilar inorganic SBU connectivity, beyond the multiple accessible proton topologies found at the surfaces of hydrated $[Zr_6O_4(OH)_4]^{12+}$ clusters.[74] For example, we are unaware of a UiO-66 polymorph containing two $[Zr_3O_2(OH)_2]^{6+}$ nodes, rather than the typical $[Zr_6O_4(OH)_4]^{12+}$ cluster. Crystal

https://doi.org/10.1021/jacs.0c10777
J. Am. Chem. Soc. XXXX, XXX, XXX–XXX

engineering to access MOF polymorphs is thus ripe for exploration because dissimilar chemical connectivity creates dissimilar electronic and physical properties (e.g., heat and electrical transport), thereby broadening the potential uses of MOFs.

2.2. Bonding Misbehaviors. *2.2.1. Metal-Centered Structural Transformations. 2.2.1.1. Dynamic Binding of Guest Molecules to Metal Sites.* Metal site geometries depicted in MOF single-crystal structures can disguise the true coordination environments of guest-filled pores. For example, although MOF-5 has served as the prototypical MOF for nearly two decades, its structure was assumed until recently to be static with idealized $Fm\bar{3}m$ space group symmetry, even in the presence of coordinating guest molecules. A combined experimental and *ab initio* molecular dynamics (AIMD) study showed that after soaking MOF-5 in *N*,*N*-dimethylformamide (DMF), one pseudo-tetrahedral Zn^{2+} ion within each Zn_4O^{6+} cluster can bind two DMF molecules, yielding a pseudo-octahedral geometry with a cluster composition of $(DMF)_2Zn_4O^{6+}$ (Figure 7).[75] Interestingly, ^{67}Zn solid-state NMR spectra of DMF-soaked MOF-5 crystals indicated the DMF interaction was random and dynamic, explaining why the crystals do not diffract until heated above the DMF boiling point. These insights provide a mechanistic rationale for phenomena such as solvent-assisted cation exchange (see below). This new MOF-5 cluster composition is also consistent with crystal structures of certain members of the IRMOF series, as well as molecular $Zn_4O(O_2CR)_6$ clusters that bind two solvent molecules per Zn^{2+} center. Variable-temperature ^{57}Fe Mössbauer spectroscopy of Fe^{2+}-doped MOF-5 later showed that temperature-dependent line broadening is observed only in the presence of N_2 but not under vacuum or Ar. This is best explained by dynamic geometrical distortions about the Fe^{2+} center[76] and shows that the MOF-5 metal centers are so susceptible to guest-induced distortions that such effects can be induced by molecules as benign as N_2.

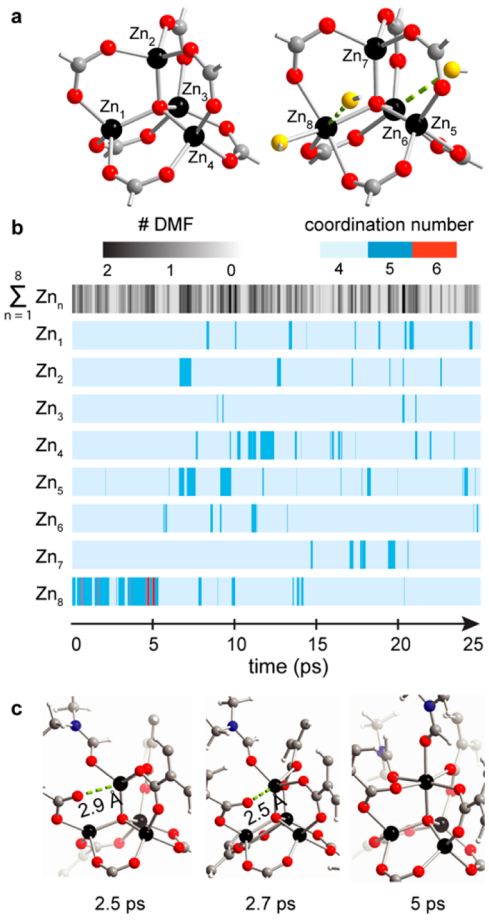

Figure 7. AIMD simulation of MOF-5 in the presence of DMF. (a) The unique Zn atoms considered in the simulation with corresponding labels. (b) Coordination number and average number of bound DMF molecules as a function of time for all eight unique Zn atoms throughout the simulation. (c) Structural representations of Zn centers taken at three representative time points.

2.2.1.2. Solvent-Induced Topological Rearrangements. Removing solvent molecules that act as placeholders in OMS coordination spheres can induce surprising structural rearrangements that imply high degrees of metal−linker dynamics. Lo et al. reported a topological reordering that occurred during a routine MOF activation procedure.[77] The as-synthesized square-lattice net is comprised of infinite Al^{3+}-carboxylate chains with DMF or other coordinating solvents serving as additional bridging linkers. Soaking in non-coordinating toluene initiates a structural reordering, affording, upon heating under vacuum, a new kagome net with much higher surface area. Inspection of this new structure revealed that its topology could only have arisen by migration of carboxylate linkers, triggered by a simple metal-centered distortion caused by displacement of bound solvent by non-coordinating toluene.

2.2.2. Post-synthetic Exchange. 2.2.2.1. Solvent-Assisted Cation Exchange. The crystalline lattices depicted by MOF X-ray structures appear rigid, but soaking many MOFs in solutions of different metal ions induces cation exchange in single crystal-to-single crystal transformations. In addition to hiding the structural flexibility, the key role of solvent in mediating metal-ion substitution is disguised. Ample evidence demonstrates the importance of solvent−metal interactions. By plotting the cation exchange rates of MOF-5 and MFU-41 versus various solvent parameters, Brozek et al. observed strong correlations with parameters that measure metal-solvent interactions, such as Gutmann donor numbers, ligand field parameter *Dq*, and metal−solvent binding enthalpies calculated by density functional theory (DFT). These correlations point to rate-limiting steps involving either solvent attack on framework metal ions, as in MFU-4l, or solvent dissociation from incoming cations, as in MOF-5.[78]

Equilibrium constants for cation exchange within a MOF are dependent on solvent. In all cases ΔS is positive and nearly solvent-independent, whereas ΔH depends on the stability of the solvated metal ions. These results meet the expectation that energetic differences among solvent-assisted mechanisms are due to differences in metal−solvent binding strength. Alternatively, entropy changes should be similar because coordinating solvents should associate and dissociate in similar proportions.[79] More generally, the crucial role of metal−solvent interactions in cation exchange was noted. For nearly all MOFs capable of cation exchange, the metal ions either are capable of higher coordination numbers to accommodate solvent attack or have solvent molecules bound to a potential OMS.[80]

2.2.2.2. Solvent-Assisted Linker Exchange. The Zr^{4+}-carboxylate bonds of UiO-66 (Figure 3) make this one of the most thermally stable MOFs. It is thus surprising that the first reports of post-synthetic linker exchange implicated them in solvent-induced cleavage of metal−linker bonds.[81] Using complementary synthetic routes, Kim et al. demonstrated that

https://doi.org/10.1021/jacs.0c10777
J. Am. Chem. Soc. XXXX, XXX, XXX−XXX

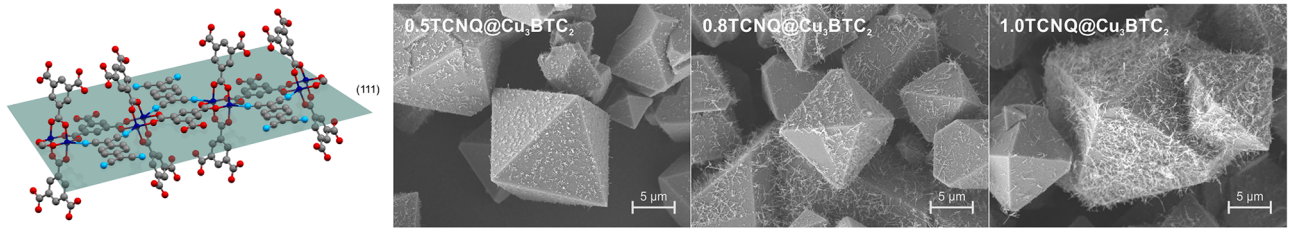

Figure 8. Left: Schematic illustration indicating TCNQ bridging two paddlewheels in $Cu_3(btc)_2$. Right: Nanowires of Cu(TCNQ) formed on the surface of $Cu_3(btc)_2$ crystals. Reproduced with permission from ref 26. Published 2018 open access by The Royal Society of Chemistry under a Creative Commons Attribution-NonCommercial 3.0 Unported Licence.

UiO-66 linkers could be replaced by linkers in solution or, even more surprisingly, by linkers from other UiO-66 particles. UiO-66 derivatives with 1,4-dicarboxylates functionalized at the 2 positions were used to probe linker exchange. For example, MOFs prepared from 2-bromo-1,4-benzenedicarboxylate were mixed with analogs built instead from 2-amino-1,4-benzenedicarboxylate. Physical mixing in the absence of solvent failed to induce linker exchange, whereas physical mixing with coordinating solvent resulted in significant exchange. Heating the bromo derivative of UiO-66 in the presence of 2-amino-1,4-benzenedicarboxylate yielded similar results. Mechanistic investigations by Marreiros et al. highlighted the role of methanol as a coordinating solvent that stabilizes defective "dangling" linkers, which exchange fastest, through H-bonding and by dynamically cleaving metal−linker bonds.[82] Such behaviors are not evident from the UiO-66 XRD structure, which obscures defects, Zr^{4+}−linker bond lability, and nuanced solvent interactions.

2.2.3. Thermal Expansion and Energy Transfer. The unit cell parameters of dense crystalline materials typically elongate with increasing temperature, but the opposite is true for MOFs. Thermal expansion coefficients α quantify the change in structural parameters, such as volumes or cell lengths. The sign of α is positive when unit cell dimensions increase with temperature, but for several well-known MOFs α is negative (negative thermal expansion, NTE). Both MOF-5[83] and $Cu_3(btc)_2$[84] display unusually large and negative α values, on the order of -10^{-5} K^{-1}. Low-energy "soft-mode" metal−linker vibrations and distortions of the metal−linker−metal vector are thought to push the structures into lower symmetry distortions. These relax into contracted framework arrangements that become magnified by increased thermal energy. Given the static picture offered by MOF X-ray structures, this behavior is surprising, as it involves a large degree of structural dynamics and flexibility.

NTE is complicated further by guest molecules. Schneider et al. demonstrated that loading pores of $Cu_3(btc)_2$ with 7,7,8,8-tetracyanoquinodimethane (TCNQ) shifted α from -16×10^{-6} K^{-1} with no TCNQ to -8×10^{-6} K^{-1} with one TCNQ per formula unit.[85] Enhancing framework stiffness by interlocking MOF clusters with bridging TCNQ was proposed to explain this trend. Similarly, Lock et al. observed that the contraction of MOF-5 cell parameters is far greater at 1.7 bar than at pressures between 5 and 150 bar, decreasing α from -15×10^{-6} to -4×10^{-6} K^{-1}.[86] Interestingly, computational models suggest that sufficiently high loadings of guest molecules can reverse the sign of α to become positive for MOFs with high guest loading levels, with the magnitude of α and its sensitivity to guest loading dependent on the particular guest molecule.[87]

Heat transport by MOFs is also influenced by guest molecules. MOF thermal conductivities are generally quite low because vacuum and porous cavities interrupt thermal energy transmitted by atomic vibrations.[88] Guest molecules would therefore be expected to enhance MOF thermal conductivity. Counterintuitively, computational modeling by Babaei et al. suggests that guest molecules in cubic frameworks with pores <1.7 nm would further reduce thermal conductivity by scattering rather than transmitting phonons.[89] Although these calculations confirm that large-pore MOFs exhibit lower thermal conductivities, the guest-induced effect is absent in larger pores due to diminished frequencies of guest collisions.

2.2.4. Guest-Induced Structural Change. Another unexpected aspect of some MOFs is their reactivity with various electron-donating molecules. Meilikhov et al. were the first to report a MOF infiltrated with a reducing agent, creating a mixed-valence charge-transfer compound, cobaltocene@MIL-47(V). This produced a surprising 12% reduction of the unit cell volume, a rare example of guest-induced formation of a mixed-valence framework.[90] An even more dramatic transformation occurs when TCNQ is adsorbed by $Cu_3(btc)_2$ in the presence of a reducing solvent such as methanol.[91] Careful experiments using a solvent-free vapor infiltration demonstrated that TCNQ bridges between two paddlewheels (Figure 8),[26] the mechanism originally proposed for the increased conductivity.[27] However, XRD and electron microscopy reveal an apparent cooperative effect, in which TCNQ reacts at the surface of $Cu_3(btc)_2$, nucleating nanowires of Cu(I)TCNQ (Figure 8). In methanolic TCNQ solution, $Cu_3(btc)_2$ thin films (<60 nm) can be fully converted to non-porous Cu(I)TCNQ,[91] an electrically conducting coordination polymer that exhibits bistable switching.[92] Subsequent work showed that intrinsic Cu(I) defects react quantitatively with TCNQ, converting them to Cu(II) and forming TCNQ radical anions.[93] This could modify the conductivity by introducing additional charge carriers into the system.

2.3. Electronic Structure Misbehaviors. *2.3.1. Mixed-Valence MOFs.* Mixed-valence MOFs (MV-MOFs) are likely candidates for electronic structure-related misbehaviors.[94] The number of MV-MOFs is growing rapidly; the topic was recently reviewed.[95] The oxidation state of the metal ions and/or linkers in MV-MOFs is not always clear, and unlike molecular complexes, a MOF crystal can have a distribution of oxidation states, as partial oxidation or reduction of the framework can occur. Here, we focus on MV-MOFs in which redox-active metal ions are the source of incongruous behavior, illustrated using the copper paddlewheel $Cu_3(btc)_2$ and Fe(1,2,3-triazolate)$_2(BF_4)_x$. These examples show that misbehaviors arising in MV-MOFs require characterization beyond XRD to determine structure−property relationships,[95] including XANES and EXAFS,[96−98]

https://doi.org/10.1021/jacs.0c10777
J. Am. Chem. Soc. XXXX, XXX, XXX−XXX

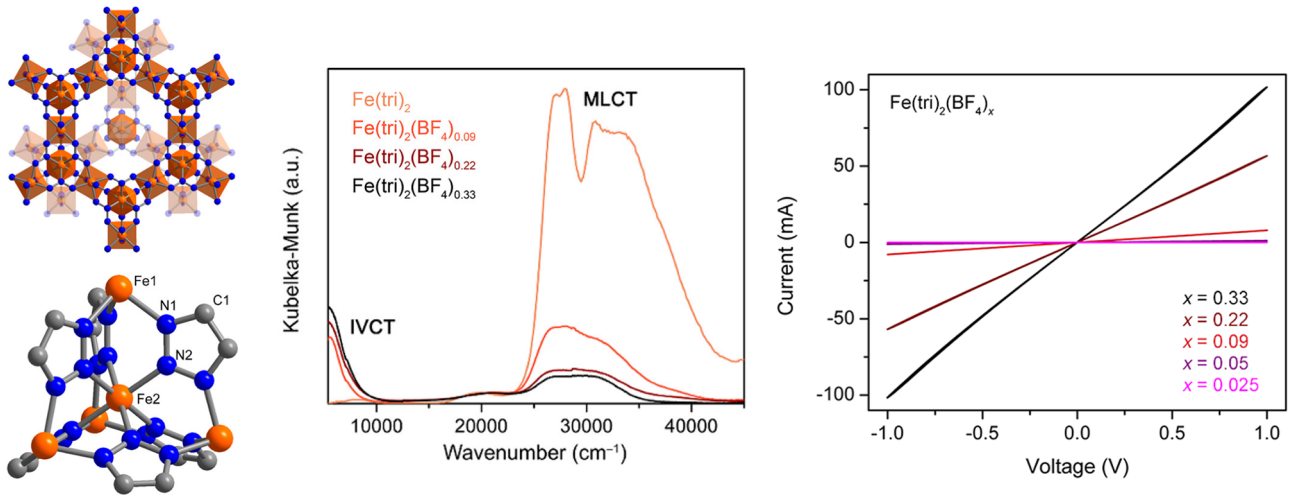

Figure 9. Fe(1,2,3-triazolate)$_2$ structure, spectra, and conductivity. Left: sub-lattice structure (top) and SBU (below), with Fe (orange), C (gray), and N (blue). Middle: Effect of oxidation on the UV−vis−IR diffuse reflectance spectrum. Right: Ohmic $I-V$ curves at room temperature. Reproduced with permission from ref 107. Copyright 2018 American Chemical Society.

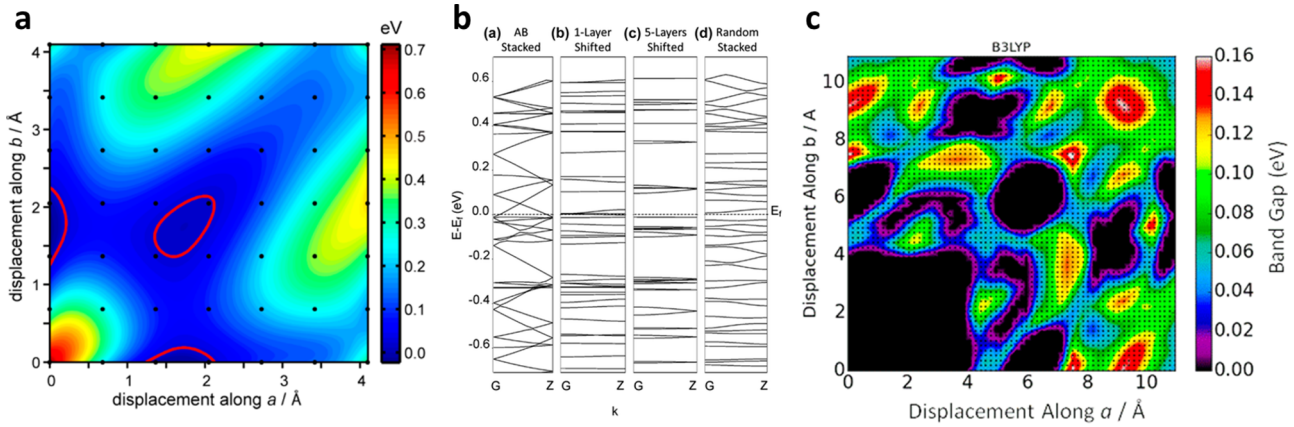

Figure 10. Electronic structure and energies of $Ni_3(HITP)_2$. (a) Map of total energy as a function of interlayer displacement. (b) Band structure plots for different stacking arrangements. (c) Map of the predicted bandgap as a function of displacement along the a and b directions. Reproduced with permission from ref 113. Copyright 2018 American Chemical Society.

electron paramagnetic resonance,[98] and chemical probe molecules in conjunction with vibrational spectroscopy.[93,96,99,100]

The primary features of $Cu_3(btc)_2$ (and copper paddlewheel MOFs in general) contributing to these misbehaviors are easily reduced Cu^{II} ions, their kinetic lability, and the propensity for missing-linker defects. Water in the pores may also play a role. It is now well established that Cu^{I} sites can form as a result of various treatments, including redox-active solvents such as methanol, heating,[101] vacuum, and soft X-rays. Some of these are either established synthetic methods or standard procedures for activating the material.[96,101−104] Even the most defect-free $Cu_3(btc)_2$ films have at least 4% reduced sites,[102] although it appears that additional washing steps during film growth can reduce their number.[105] Charge balancing requires a Cu−linker bond to be broken (in the absence of cations in the pores), creating missing-linker defects.[93] Their formation may be facilitated by the different preferred coordination geometries of Cu^{II} (square pyramidal) and Cu^{I} (tetrahedral). The mixed-valence behaviors exhibited by $Cu_3(btc)_2$ are likely found in other copper paddlewheel MOFs, but the only one reported is a structure assembled from thiophene(bis-triazole)dibenzoate linkers.[106]

In contrast to $Cu_3(btc)_2$, Fe(1,2,3-triazolate)$_2(BF_4)_x$ ($0 \le x \le 0.33$) is a 3D MV-MOF that exhibits an intervalence charge-transfer band in the IR (5000−10000 cm^{-1}) that is diagnostic for partial oxidation (Figure 9).[107] A continuous range of oxidation states is accessible, and the material is highly sensitive to post-synthetic oxidation, which was not initially suspected. The basic structure is maintained upon oxidation, although the unit cell contracts slightly. However, extremely large variations in the electrical conductivity occur (Figure 9). Initially, a conductivity of 7.7×10^{-5} S/cm was reported for the fully reduced state.[108] Subsequently, a much lower value (7×10^{-9} S/cm) was reported following rigorous exclusion of air from the sample.[107] In contrast, chemical oxidation of the fully reduced material to a mixed-valent Fe^{II}/Fe^{III} structure increases the conductivity by a factor of 10^8 and is accompanied by a decrease in surface area with increasing MV character due to charge-balancing anions in the pores. The results emphasize that special caution must be exercised in studies of the CT properties of MV-MOFs, as even small valence impurities can have a dramatic effect on the conductivity.

2.3.2. Stacking Disorder in 2D MOFs. In contrast to 3D-connected MOFs, the forces holding together the layers of 2D MOFs are rather weak, allowing a large number of stacking

https://doi.org/10.1021/jacs.0c10777
J. Am. Chem. Soc. XXXX, XXX, XXX−XXX

arrangements to have similar energies. This makes it difficult to obtain single crystals suitable for XRD.[109−111] It also produces misbehaviors in the form of disagreements between predicted and measured electronic structure properties. A noteworthy example is $Ni_3(HITP)_2$ (HITP = 2,3,6,7,10,11-hexaiminotriphenylene),[112] which consists of π-stacked layers of Ni^{2+} ions coordinated to amine groups to form sheets with the same topology as graphene. Eclipsed and slipped-parallel structures cannot be distinguished by powder XRD. Although DFT calculations predict that the slipped-parallel structure is the most stable,[112] structures displaced by as much as 3 Å along either the *a* or *b* unit cell direction have essentially the same energy (Figure 10a).[113] It is likely, therefore, that the bulk material is comprised of layers displaced from each other in the *xy* plane randomly by varying amounts. This affects the band structure (Figure 10b) and bandgap (Figure 10c), transforming a material expected by theory to be metallic (AB stacked) to a narrow bandgap semiconductor (one or more layers shifted; Figure 10b).

3. GAS STORAGE

3.1. Adsorbate Adaptive Pore Spaces. Whereas the effects of MOF framework flexibility on gas storage properties have been well established over the past two decades,[10] computational assessment of porous materials has relied on the rigid structure approximation. This is likely due to the complexity and cost associated with atomistic simulations that rigorously couple unrestricted framework dynamics with adsorption in an open system.[114] MOFs with dynamic linear chains provide opportunities to observe how a framework responds to adsorbates,[115] which in turn affects gas storage properties. For example, Witman et al. rigorously coupled framework dynamics and adsorption to show a significant increase in methane deliverable capacity (~20%) in thioether-functionalized MOF-5[116] compared with a simulation with frozen side chains.[21] Subtle reorganization of the side chains cooperatively reduces the accessible pore volume, and thus uptake, at low chemical potentials. These insights suggest that functionalizing MOFs to produce adaptive pore sizes is an alternative to seeking rigid MOFs with very small pores for weakly interacting gases such as H_2 and CH_4.[18,117]

3.2. Open Metal Site Distortion for Enhanced H_2 Binding. Whereas the original MOF-74 was synthesized with formula unit M_2(dobdc) (M = Mg, Mn, Fe, Co, Ni; $dobdc^{4-}$ = 2,5-dioxido-1,4-benzenedicarboxylate), a structural isomer can be synthesized with the regioisomeric *m*-dobdc (*m*-$dobdc^{4-}$ = 4,6-dioxido-1,3-benzenedicarboxylate) linker. The two isomers both exhibit a honeycomb lattice with nearly identical geometric pore properties. The octahedral OMSs, formed from 1D-rod metal oxide SBUs, are at first glance also identical. Surprisingly, the hydrogen storage properties of M_2(*m*-dobdc) are significantly better than those of M_2(dobdc), with an H_2 binding enthalpy increased by 0.4−1.5 kJ/mol for various M.[118] Detailed characterization showed that the binding distance between the exposed M^{2+} OMS and H_2 is shorter in M_2(*m*-dobdc), a consequence of higher charge density on the M^{2+} cation produced by a subtle distortion of its octahedral coordination environment.[19] Thus, coordination environment modification represents a second strategy for improving uptake of weakly interacting gases. For example, anion exchange of bridging ligands in an OMS-MOF significantly improved O_2 affinity, despite the metal center, coordination geometry, and framework topology remaining unchanged.[119]

3.3. Adsorbate-Induced Symmetry Breaking. The iconic and easily recognized hexagonal honeycomb lattice of CPO-Mg-27 (more commonly referred to as MOF-74 or IRMOF-74) is one of the best-studied MOFs. The material can be expanded in an isoreticular series with pores as large as 98 Å.[120] Ar adsorption at 87 K by IRMOF-74-V-hex exhibits an unusual small-angle X-ray scattering (SAXS) pattern that suggested the formation of extra Ar domains in the mesopores.[121] Jawahery et al. formulated an alternative explanation for the SAXS pattern and, using molecular simulations, demonstrated an adsorbate-induced symmetry breaking of the honeycomb lattice over multiple unit cells (Figure 11).[17] This phenomenon is observed outside the MOF-

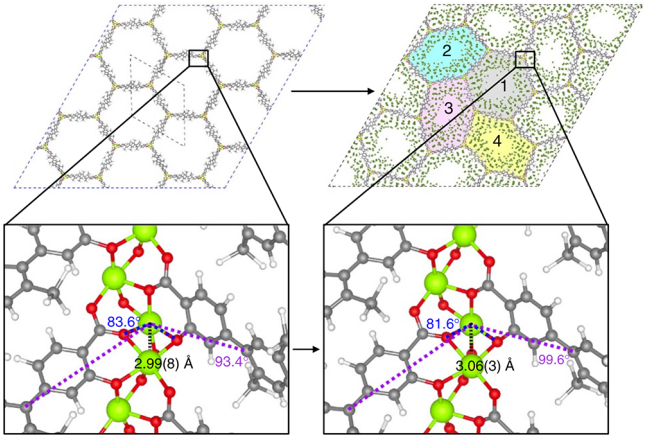

Figure 11. Experimentally observed SAXS profiles in the 87 K, Ar-loaded IRMOF-74-V-hexagonal structure can be explained by symmetry breaking of the idealized honeycomb lattice. Reproduced with permission from ref 17. Copyright 2017, The Author(s), published open access by Springer Nature licensed under the terms of the Creative Commons CC BY license.

74 system as well, including $Cu_3(btc)_2$.[26] Such complex deformation patterns have significant implications for MOF-74 applications beyond gas storage, as discussed later in this Perspective.

3.4. Reduced Mechanical Stability from Pre-distorted Linkers. High MOF mechanical stability is critical for practical applications in gas storage systems in which the charging pressures necessitated by technical storage targets can reach 65 or 100 bar for methane and hydrogen, respectively.[122] Redfern et al. recently correlated the bulk modulus of MOFs with quantities such as void fraction and linker length,[123] finding in several cases that measurements deviated significantly from the correlations. It was discovered that the crystal structure of the anomalies contained "pre-distorted" linkers in the absence of external pressure. This was sufficient to reduce the rigidity of the framework compared with other structures with similar void fraction and linker length (Figure 12). This insight provides a leading indicator of reduced mechanical stability and thus reduced suitability for practical gas storage applications.

4. CHEMICAL SEPARATIONS

4.1. Dynamic Pore Size Distribution Broadening. Even in the absence of obviously flexible moieties within a MOF, the pore size distribution (PSD) described by the idealized crystal structure (i.e., DFT-minimized or experimentally resolved single-crystal structures) may not be representative of the actual PSD. The PSD broadens and its mean can shift at finite

https://doi.org/10.1021/jacs.0c10777
J. Am. Chem. Soc. XXXX, XXX, XXX−XXX

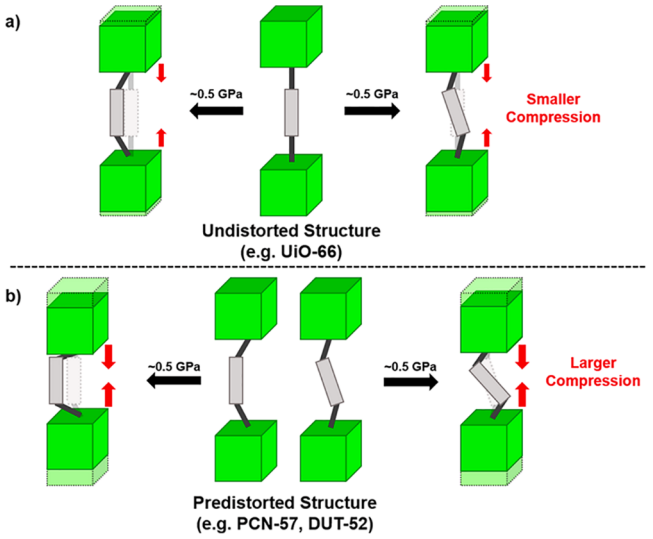

Figure 12. Schematic illustrating the effect of linker distortion on MOF mechanical stability. Reproduced with permission from ref 123. Copyright 2019 American Chemical Society.

temperatures, despite a constant unit cell volume. Even if small in magnitude, this has significant implications for chemical separations. For example, rigid simulations of Xe/Kr separation by SBMOF-1, which holds the record selectivity, overestimate this behavior,[124] in part because finite temperatures decrease the mean PSD by ~0.5 Å.[20] This result is a general one that systematically affects the Xe/Kr Henry regime selectivity across hundreds of MOF materials. Although not a design strategy as such, awareness of this should improve the accuracy of high-throughput screening studies aimed at identifying optimal materials for shape-selective separations such as CH_4/CO_2.

4.2. Xylene Separation Enhancement. Similar to the IRMOF-74-V-hex example above, M_2(dobdc) can also undergo a deformation in response to adsorption that breaks the symmetry of its honeycomb lattice. Interestingly, this deformation pattern only occurs with M = Co and *o*-xylene or ethylbenzene as the adsorbate.[22] Whereas the undistorted channels can only adsorb three *o*-xylene molecules per six OMSs, adsorption-induced distortion in three out of four channels allows four *o*-xylene molecules to adsorb per six OMSs. This unusual selectivity results from the ability of some xylene isomers to interact with two adjacent OMSs (Figure 13), revealing an unexpected design strategy for shape-selective adsorption and separation.

4.3. Modulating the Step for Cooperative CO_2 Adsorption. MOFs have attracted significant attention for their potential to separate CO_2 from flue gas; thus, it was a significant breakthrough when it was demonstrated that CO_2 could cooperatively insert into the diamine-appended mmen-M_2(dobpdc) (mmen = *N*,*N*′-dimethylethylenediamine, dobpdc^{4-} = 4,4′-dioxidobiphenyl-3,3′-dicarboxylate) framework (Figure 14).[125] The practical utility of the material for

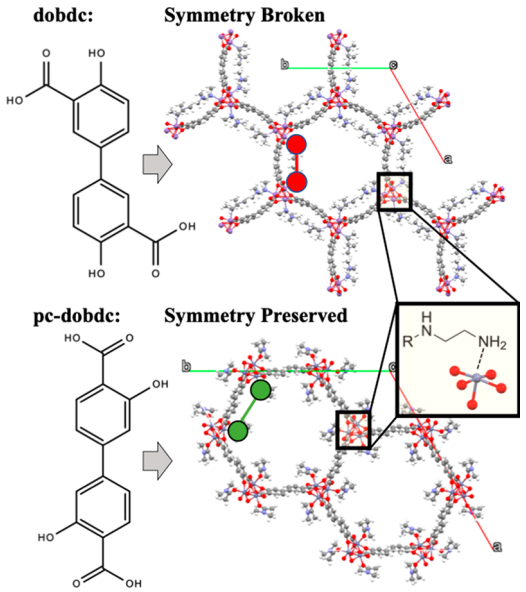

Figure 14. Diamine insertion at the open metal site in expanded MOF-74 analogs (inset) permits cooperative CO_2 adsorption and step-shaped isotherms. Substitution of R with bulkier alkyl groups results in undesired double-stepped isotherms in the M_2(dobpdc) framework, but not M_2(pc-dobpdc), because linker buckling reduces the honeycomb lattice symmetry. This in turn forces adjacent diamine chains into closer proximity in the *ab* plane and increases their steric hindrance.

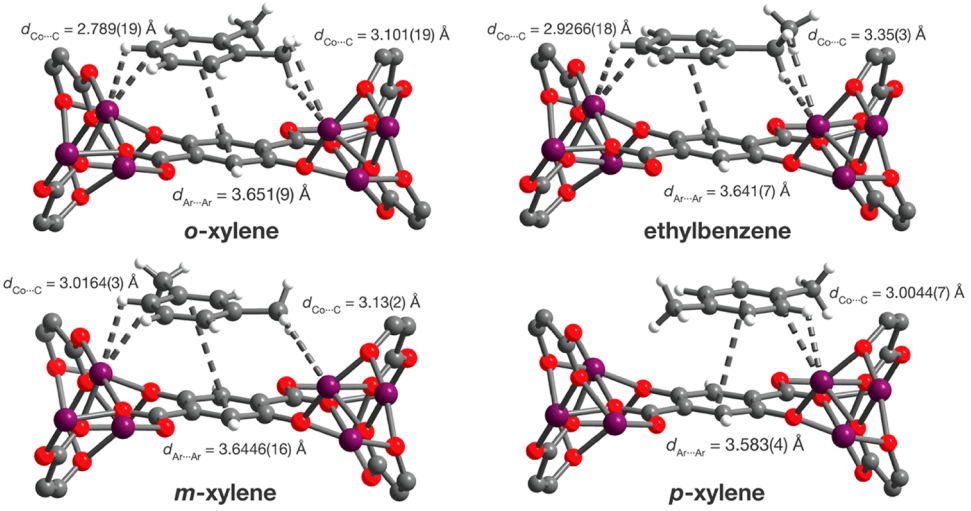

Figure 13. Bond distances of xylene isomers in Co_2(dobdc). Reproduced with permission from ref 22. Copyright 2018 American Chemical Society.

https://doi.org/10.1021/jacs.0c10777
J. Am. Chem. Soc. XXXX, XXX, XXX−XXX

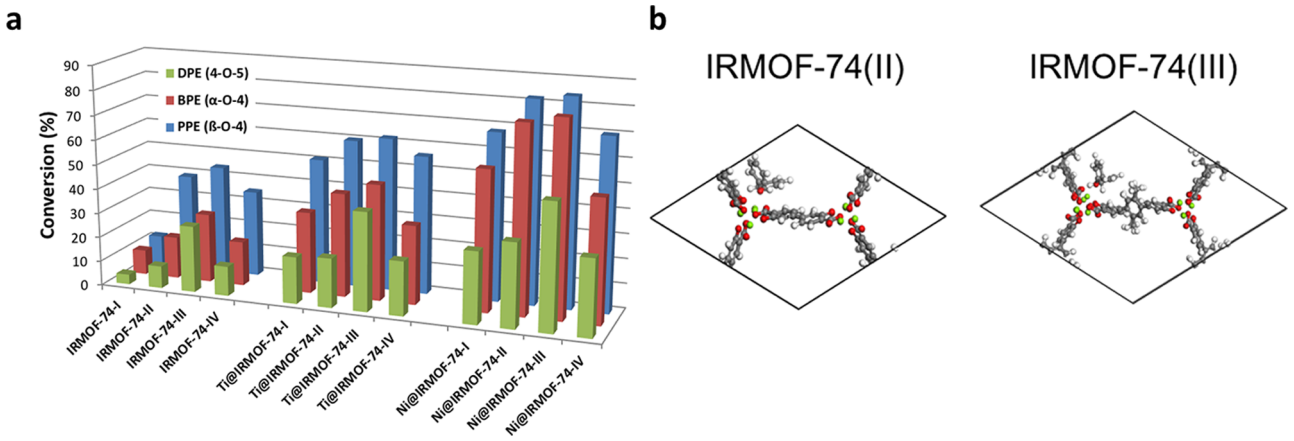

Figure 15. (a) Hydrogenolysis conversion of three aryl ethers by IRMOF-74-*n*. (b) Preferred orientation of MOF linker and diphenyl ether substrate with respect to the Mg^{2+} OMS in IRMOF-74(II) and IRMOF-74(III) as predicted by DFT. Reproduced with permission from ref 25. Published open access by The Royal Society of Chemistry under a Creative Commons Attribution-NonCommercial 3.0 Unported Licence.

real-world applications depends on where and how the resulting step-shaped CO_2 isotherm occurs. Diamine attachment at the OMS is shown schematically in the Figure 14 inset. Varying the diamine R group affects the CO_2 adsorption thermodynamics.[24] Appending a single methyl group results in an undesired and performance-limiting double step in the CO_2 adsorption isotherm of M_2(dobpdc) but not that of the M_2(pc-dobpdc) analog (pc-dobpdc^{4-} = 3,3′-dioxidobiphenyl-4,4′-dicarboxylate, pc = para-carboxylate). This occurs because steric hindrance between adjacent diamine chains in the *ab* plane is amplified when linker buckling disrupts the hexagonal lattice of M_2(dobpdc), forcing adjacent diamine chains into close proximity. This buckling is absent in M_2(pc-dobpdc), however, ensuring that diamine chains remain equidistant in the *ab* plane and bulkier R group substitutions do not induce a double step in the CO_2 isotherm. Once again, a subtle symmetry breaking of the idealized honeycomb lattice is required to rationalize and predict complex gas adsorption behavior.

5. CATALYSIS AND REACTIVITY

5.1. Increased Reactivity from OMS Distortion. The recognition that the archetypal honeycomb lattice of MOF-74 can distort, albeit slightly, also has implications for catalytic reactivity. For example, Stavila et al. demonstrated that the IRMOF-74-*n*(Mg) (*n* = I− IV) series catalyzes the hydrogenolysis of aryl ether bonds.[25] The non-monotonic catalytic activity trend was surprising (Figure 15a) and was rationalized by DFT modeling. This showed that, unique among the four MOFs, the Mg(II) OMS of IRMOF-74(III) is displaced toward the pore interior. Apparently, this is caused by rotation of the middle ring of the IRMOF-74(III) linker (Figure 15b) to minimize steric hindrance between methyl groups added to increase linker solubility. The resulting higher substrate binding energy compared to IRMOF-74-II caused by this subtle chemical change represents a misbehavior relative to that expected from an invariant isoreticular topology. Although unexpected, this raises a possible new design strategy, whereby the catalytic properties of an OMS center can be enhanced by tuning internal rotation through linker functionalization.

5.2. Catalysis Enabled by Disguised OMS. Heterogeneous catalysis involving bond formation and charge transfer with substrates requires metal centers with accessible coordination sites, as in the limited classes of MOFs with OMS. Examples include the M-MOF-74 and M-BTT (BTT= 1,3,5-benzenetristetrazolate) MOF families, whose single-crystal structures exhibit coordinated but removable solvent molecules. However, some MOFs have "disguised" OMSs that allow them to catalyze such reactions even though they apparently lack OMS. For example, although the single-crystal structure of MIL-47 indicates that the vanadyl centers are coordinatively saturated, this MOF catalyzes selective epoxidation of cyclohexene.[126] Mechanistic investigations indicate that, whereas water, a coordinating solvent, leaches vanadium ions that could account for a portion of the observed catalytic activity, decane, a non-coordinating solvent, enhances catalytic selectivity and recyclability. These experiments and modeling support mechanistic pathways that invoke dynamic dissociation of terephthalate linkers from the vanadyl coordination sphere, allowing substrate to bind.[127] Recent studies have shown that linkers dynamically dissociate from metal centers in carboxylate-based MOFs in general. The general lability of metal−carboxylate bonds therefore suggests that MOFs without OMSs may well be attractive for heterogeneous catalysts.

Another form of disguised OMS can occur at metal centers that can achieve higher coordination numbers than depicted in the single-crystal structure. Just as the nominally four-coordinate metal centers of the IRMOF series can achieve five- or six-coordinate geometries, the metal centers in the M-MFU-4l[128,129] and related M-CFA-1[130,131] families shuttle through high-coordinate species, even though their single-crystal structures show pseudo-tetrahedral geometries. For example, following nucleophilic attack of CO_2, the originally four-coordinate Zn-OH species of Zn-CFA-1 adopts a five-coordinate geometry with bound carbonate.[130] Similarly, the pseudo-tetrahedral Ni-Cl centers of Ni-MFU-4l and Ni-CFA-1 pass through five-coordinate intermediates of a Cossee−Arlman-type mechanism while catalyzing the selective dimerization of ethylene to form 1-butene.[128,131] The apparent ability of MFU-4l to accommodate metal sites with higher coordination numbers than as depicted in the original single-crystal structures inspired their use in polymerization catalysis by employing variants with five-coordinate $TiCl_2$ and $CrCl_2$ and pseudo-octahedral VCl_3 metal centers.[132,133] These examples demonstrate that all possible coordination numbers of MOF metal sites should be considered when selecting potential catalysts,

https://doi.org/10.1021/jacs.0c10777
J. Am. Chem. Soc. XXXX, XXX, XXX−XXX

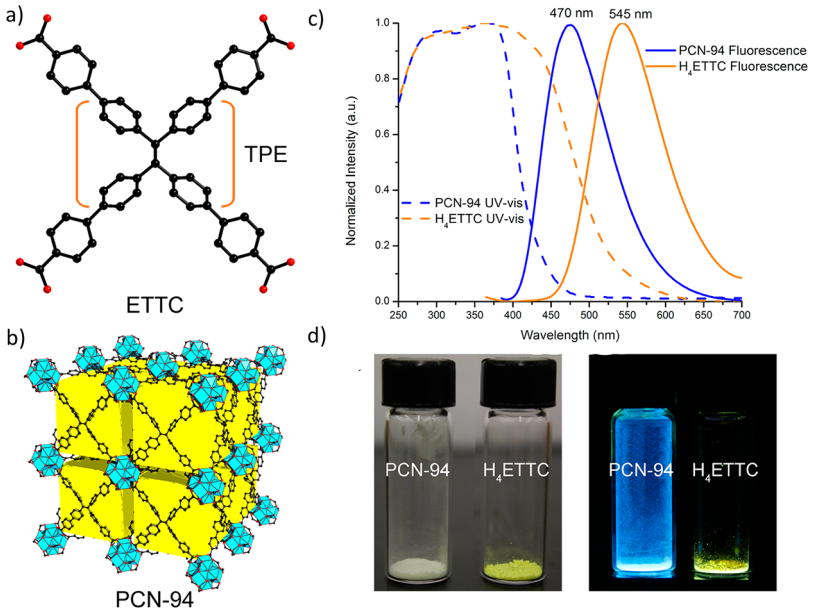

Figure 16. Luminescent PCN-94: (a) (Ethene-1,1,2,2-tetrayl)tetrakis([1,1′-biphenyl]-3-carboxylate) (ETTC) linker. Orange brackets indicate the luminescent tetraphenylethylene core. (b) PCN-94 framework. (c) Solid-state absorption and emission spectra. (d) PCN-94 and H_4ETTC shown under ambient (left) and UV (right) light. Reproduced with permission from ref 150. Copyright 2014 American Chemical Society.

especially MOF families that include pseudo-tetrahedral Zn^{2+}, which readily assumes high coordination.

6. ELECTRONIC STRUCTURE PROPERTIES

6.1. Intrinsically Conducting MOFs. Most MOFs are poor electrical conductors, and the mechanisms behind their charge transport are not well understood, although a high-level categorization into hopping versus band transport has been suggested.[134,135] MOF nanoporosity is seemingly in opposition to high electrical conductivity, as this isolates the structural elements, in particular the organic linkers that could provide a pathway for charge transport. For example, porous MOFs based on the TCNQ linker have been reported but are not known to be conducting.[136] However, dense CPs Cu(TCNQ)[92] and Tl-(TCNQ)[137] are conducting. In general, electrical conductivity depends on the sign of the charge carrier, the concentration of charge carriers, and their mobility. Data of this nature for MOFs are sparse, which inhibits understanding needed to design conducting frameworks. For example, charge carrier mobilities have been reported for only a handful of MOFs.[135]

Narrow band gaps are another signature of electrical conductivity, as these affect the Boltzmann population of charge carriers. Although the wide band gaps typical of MOFs can be readily tuned,[34,138] the highly localized nature of the charge carriers is considerably more difficult to overcome. Moreover, the supramolecular and structurally flexible nature of MOFs contributes to unexpected bandgap behaviors. For example, the band gap of MIL-53-type MOFs can change by >1 eV as a result of breathing modes induced by guest-molecule uptake.[139] More subtly, SBUs that are nominally presumed to be electronically isolated, as in $Cu_3(btc)_2$, exhibit communication between units that must be invoked to explain excitation spectra.[140] Rational design of conductive MOFs would thus benefit from a microscopic understanding of the charge transport mechanisms, but such insight has been elusive in many prominent conductive MOFs. These examples demonstrate that the electronic structure of a given MOF cannot be assumed to remain stable. Consequently, misbehaviors in charge transport properties should be expected if conventional organic and inorganic conductors define the baseline for comparison.

6.2. Guest-Modulated Electrical Conductivity. Introducing guest molecules within MOF pores can lead to unexpected charge transport behaviors compared with activated material. A primary example is guest-induced modulation of electrical conductivity. This was first discovered in $Cu_3(btc)_2$ infiltrated with redox-active TCNQ (Figure 8), converting this MOF from a dielectric material to an electrical conductor (conductivity increased by at least a factor of 10^8) without any change to the crystal structure.[27] Water adsorption by $Cu_3(btc)_2$ provides a second example, demonstrating that non-redox-active molecules binding to the OMS can modify the bandgap and potentially the charge transport properties. A long-standing mystery is the origin of the color change in $Cu_3(btc)_2$ induced by adsorption of water by the activated MOF. One hypothesis is that partial reduction creates (Cu^{II}–Cu^{I}) dimers with a missing linker. The consequent removal of the center of symmetry eliminates the Laporte selection rule, making the forbidden d-d transitions fully allowed.[105] This "retrofitting" strategy[40,85,93,141] has great potential for conductivity tuning/enhancement, but the range of guest molecules employed is still limited.[135] For example, we recently pointed out that guest-loaded MOFs could be used as memristors.[142] Guest loading, redox potential, and ion diffusivity can all be used to modulate the resistivity of the conducting channel.

A major motivation for constructing electrically conductive MOFs is their application to create high-surface-area recognition chemistries for sensing. There are numerous examples of chemiresistive sensors employing changes in charge transport to detect analytes.[142] However, charge transport depends on several physical parameters, the effects of which on the electronic conductivity can be unpredictable. For example, a 2D conducting MOF analogous to the $Ni_3(HITP)_2$ scaffold features a turn-off response in the presence of CO_2; i.e., the conductivity decreased with increasing CO_2.[143] Spectroscopy

https://doi.org/10.1021/jacs.0c10777
J. Am. Chem. Soc. XXXX, XXX, XXX−XXX

and band structure calculations suggest this apparent misbehavior results from free carrier absorption by CO_2, a surprising behavior considering CO_2 is neither a dopant nor redox active.

6.3. Stimuli-Responsive Luminescent Frameworks. Turn-on and turn-off luminescence in response to chemisorption is a difficult MOF property to predict. Luminescence stimulated by ionizing radiation is a related example.[144] A misbehavior arises when the photophysical properties of a fluorophore are not observed once it is incorporated into the scaffold. Luminescence quenching by guest adsorption (i.e., a turn-off response) is observed for many natively emissive MOFs[145] and is readily explained by alignment of guest unoccupied orbitals with the MOFs conduction band. For example, highly electron-deficient aromatics can act as electron traps for fluorescent linkers.[146,147] However, incongruities exist. For example, a series of MOF-74 analogues with 4,4′-bipyridine linkers exhibits both linker-centered and ligand-to-metal charge-transfer luminescence. Both quenching and enhancement are observed in the presence of dissimilarly functionalized aromatic guests.[148] It is unclear whether close alignment of the linker unoccupied orbitals with the MOF conduction band governs the response or something more subtle. The guest−MOF band alignment mechanism can be applied to non-aromatic molecules with an accessible LUMO (e.g., CS_2), but internal electron transfer is a limited strategy for designing a turn-off response.[149] Turn-on luminescence is particularly intriguing because the MOF structure suppresses or enhances a property otherwise active in its free molecular constituents. The structure−property relationships are difficult to discern but are influenced by MOF structure at all levels.[144] The response stems from competition between the favorable crystal cohesion energy and the chromophore distortion energetic penalty. For example, a MOF lattice can rigidify a luminescent ligand (Figure 16)[29,150] or constrain a guest,[151] increasing the quantum yield to virtually 100%.[150] MOFs that stabilize a fluorophore in a dark geometry can become luminescent when external stimuli induce a structural transition (non-obvious from the crystal structure), enhance interlinker π-overlap,[152,153] or enable bond-forming reactions with the linkers. These can be used to tune the selectivity of the turn-on response.[154−156] Such complex interrelationships point to the necessity for computational modeling to understand alignment between MOF bands and guest molecular orbitals and the effects on fluorophore rigidity and vibrational modes due to incorporation in the MOF crystal. However, with so few examples of novel turn-on and turn-off incongruities, there is also a need for further fundamental synthetic endeavors to guide theory.

7. SUMMARY AND OUTLOOK

The foregoing discussion shows that unexpected behaviors can result from even very subtle factors that invalidate the assumptions described in section 2. What is particularly remarkable is that examples of unexpected behavior are still being uncovered in some of the most intensely investigated MOFs, such as MOF-5, $Cu_3(btc)_2$, and MOF-74, decades after their initial discovery.

In brief, we identified several MOF structural elements that signal the possibility of unexpected behaviors. Foremost among these are structural and kinetic aspects related to the linkers. Linker kinetic lability can allow more than one coordination geometry to be present or accessible for the same metal oxidation state. Linkers that rotate or distort upon incorporation within the framework (sections 2.1, 3.3, and 3.4), have flexible side chains (section 3.1), or undergo dynamic dissociation (section 5.2) can lead to non-monotonic property variation within the series. This can alter OMS reactivity (section 5.1) and separation selectivity (sections 4.1 and 4.2). Pore sizes close to adsorbate dimensions can induce non-intuitive gas uptake and separation behaviors (sections 3.1 and 4.1). Metal ions also produce unexpected behaviors due to redox-active nodes (section 2.3.1), distortion of the OMS environment (section 5.1), and expandable coordination shells (section 5.2). At the supramolecular level, difficult-to-predict weak interactions, such as inter-layer forces (section 2.3), can lead to materials with dramatically different electronic properties (sections 2.3.2 and 6.1). Finally, phenomena induced by external stimuli (section 6.3), such as pressure, electric fields, and guest molecules (sections 6.2 and 6.3), are among the most difficult to anticipate. These are the most prominent examples we are aware of, but there are aspects of MOFs that are currently so poorly understood that it is impossible to say what is misbehavior and what is not.

These observations by no means invalidate the fundamental concepts that give rise to MOFs and lead to rational design principles. On the contrary, the exceptional degree of structural control possible in MOFs creates the possibility that the misbehaviors and incongruities discussed here can be harnessed to address some of the many challenges facing the field. Consequently, the outlook is bright for developing new strategies in several major application spaces. In addition to the possibilities highlighted above, we see key opportunities in these areas:

(1) *Gas storage and separations.* Solving the difficult problem of storing weakly interacting gases such as hydrogen and methane under ambient conditions may require going beyond the search for structures with a high volumetric density of OMS. An alternative strategy is to seek structures having very small pores—on the order of the molecular kinetic diameter—to boost the isosteric heat of adsorption. However, even a nominally non-porous structure may undergo a non-porous-to-porous transition (at *constant* unit cell volume) driven by high adsorbate binding energies, making it exceedingly difficult to identify this unexpected feature.[20,157] The enormous number of MOF structures provides a basis for optimism, as these can enable high-throughput screening[158] and machine learning[159] to identify subtle structure−property relationships. However, the success of high-throughput screening depends on the availability of accurate potentials for OMS and other strong-binding sites. Moreover, flexible structures can only be identified if both framework dynamics and adsorption are included—capabilities beyond virtually all available high-throughput methods. Analytical models have shown promising signs that such materials could exist, but this remains to be shown experimentally.[20,21]

(2) *Catalysis and reactivity.* An important finding here is that seemingly very similar structures can exhibit reactivity patterns that differ in significant but unexpected ways, such as discussed above for IRMOF-74(n).[25] One of the most interesting challenges therefore (and greatest opportunities) in MOF catalysis is to predict how these subtle structural modifications affect reactivity. The effect on the OMS coordination environment (and hence,

https://doi.org/10.1021/jacs.0c10777
J. Am. Chem. Soc. XXXX, XXX, XXX−XXX

reactivity) of groups that solubilize linkers has been largely overlooked. Recently it was shown that MOF-5's thermal stability is reduced by methyl functionalization.[160] A reexamination of existing MOFs is warranted to identify other examples in which a structural modification made far from the active site changes the catalytic activity. This must be coupled with a concerted synthetic effort to determine structure−property relationships, which could provide the basis for new isoreticular series to modulate reactivity. Novel solubilization strategies could also result, such as the linker salt approach,[161] to avoid unanticipated effects due to linker functionalization.

(3) *Charge transport.* Although the MOFs with the highest electronic conductivity are 2D layered structures that suffer from intralayer disorder, new understanding gained from conductivity measurements on single crystals,[109,110] data on charge mobility (although still very limited),[135] and high-level theoretical approaches are defining strategies for controlling this disorder.[162,163] Moreover, recently reported lanthanide-based MOFs demonstrate that high conductivity can be achieved by using interlayer spacers to create ordered 3D structures exhibiting one-dimensional charge transport.[111] Remarkably, it appears that substantial improvements in the charge transport properties of nominally insulating MOFs are feasible.[164] As the vast majority of MOFs are 3D structures but are expected to be insulating, this represents a promising new research direction with the potential to create a much larger class of porous conducting MOFs. An added incentive is that 3D structures are typically more crystalline than the highly conducting but disordered 2D layered structures, suggesting that the conductivity of 3D materials will be less affected by defects. As the properties of MOF films used in electronic devices play such an important role in device behavior, the revelation that linker sterics (e.g., the hindered rotation in PCN-14[45]) can affect film microstructure suggests this as a novel strategy to control a property for which few structure−property relationships exist.

(4) *Mechanical properties.* Compared with other MOF properties, their counterintuitive NTE has received relatively little attention. Recent work is revealing the underlying mechanisms of this behavior,[165] and general strategies are emerging,[85,166−168] including the effects of rotatable linker groups[169] and solvent molecules.[168] Two promising opportunities are the use of strain-based microcantilever sensors and gas storage. Chemical detection using MCL has been demonstrated,[170] but optimizing mechanical properties to increase adsorbate-induced strain should improve sensitivity.[171] To increase the deliverable capacity of MOF-based sorbents, an intriguing possibility is to couple NTE with a non-porous-to-porous transition in a pressure−temperature swing adsorption cycle.

(5) *Stimuli-responsive MOFs.* Turn-on luminescence is of considerable interest, given the large number of potential applications.[152] Although mechanistic understanding is limited, the growing research effort and numerous luminescent MOFs will likely lead to structure−function relationships. In contrast, MOFs that respond to stimuli other than photons are much rarer. Intrinsically electroluminescent MOFs are of great interest for white light LEDs, but only a few are known.[172−177] Pyroelectricity is also a little-explored effect,[178−180] although there are many ferroelectric MOFs.[181] Pressure can produce some highly non-intuitive responses, including negative gas adsorption,[69] for which structure−property relationships only recently emerged.[182,183] The very limited understanding of these phenomena highlights the difficulty of classifying them as misbehaviors, although their very rarity suggests that chemists have not yet learned how to engineer these properties into MOFs.

In conclusion, we believe that, far from diminishing the appeal of MOFs as a class of materials, these "exceptions to the rules" do just the opposite. Development of fundamental understanding and structure−property relationships eventually will make these less mysterious. Our hope is that highlighting them here will stimulate unorthodox viewpoints, leading to both deeper fundamental understanding and exciting new MOF applications. Keeping in mind that "What you see is *not* always what you get" will certainly be essential to fully understand these materials and maximize their potential.

AUTHOR INFORMATION

Corresponding Author

Mark D. Allendorf − *Chemistry, Combustion, and Materials Science Center, Sandia National Laboratories, Livermore, California 94551, United States;* orcid.org/0000-0001-5645-8246; Email: mdallen@sandia.gov

Authors

Vitalie Stavila − *Chemistry, Combustion, and Materials Science Center, Sandia National Laboratories, Livermore, California 94551, United States;* orcid.org/0000-0003-0981-0432

Matthew Witman − *Chemistry, Combustion, and Materials Science Center, Sandia National Laboratories, Livermore, California 94551, United States;* orcid.org/0000-0001-6263-5114

Carl K. Brozek − *Department of Chemistry and Biochemistry and Oregon Center for Electrochemistry, University of Oregon, Eugene, Oregon 97403, United States;* orcid.org/0000-0002-8014-7904

Christopher H. Hendon − *Department of Chemistry and Biochemistry, University of Oregon, Eugene, Oregon 97403, United States;* orcid.org/0000-0002-7132-768X

Complete contact information is available at: https://pubs.acs.org/10.1021/jacs.0c10777

Notes

The authors declare no competing financial interest.

ACKNOWLEDGMENTS

M.D.A., V.S., and M.W. gratefully acknowledge the support of the Sandia Laboratory Directed Research and Development (LDRD) Program and the Hydrogen Materials-Advanced Research Consortium (HyMARC), established as part of the Energy Materials Network under the U.S. Department of Energy, Office of Energy Efficiency and Renewable Energy, Hydrogen and Fuel Cell Technologies office, under Contract No. DE-AC04-94AL85000. C.K.B. gratefully acknowledges the University of Oregon for generous startup funds. C.H.H. acknowledges the National Science Foundation Division of Materials Research under grant no. DMR-1956403 for supporting a portion of this work. Sandia National Laboratories is a multimission laboratory managed and operated by National

https://doi.org/10.1021/jacs.0c10777
J. Am. Chem. Soc. XXXX, XXX, XXX−XXX

Technology and Engineering Solutions of Sandia, LLC., a wholly owned subsidiary of Honeywell International, Inc., for the U.S. Department of Energy's National Nuclear Security Administration under contract DE-NA-0003525.

REFERENCES

(1) Furukawa, H.; Cordova, K. E.; O'Keeffe, M.; Yaghi, O. M. The Chemistry and Applications of Metal-Organic Frameworks. *Science* **2013**, *341*, 1230444.
(2) Eddaoudi, M.; Kim, J.; Rosi, N.; Vodak, D.; Wachter, J.; O'Keeffe, M.; Yaghi, O. M. Systematic Design of Pore Size and Functionality in Isoreticular MOFs and Their Application in Methane Storage. *Science* **2002**, *295*, 469−472.
(3) Oien-Odegaard, S.; Shearer, G. C.; Wragg, D. S.; Lillerud, K. P. Pitfalls In Metal-Organic Framework Crystallography: Towards More Accurate Crystal Structures. *Chem. Soc. Rev.* **2017**, *46*, 4867−4876.
(4) Li, H.; Eddaoudi, M.; O'Keeffe, M.; Yaghi, O. M. Design and Synthesis of An Exceptionally Stable and Highly Porous Metal-Organic Framework. *Nature* **1999**, *402*, 276−279.
(5) Sillar, K.; Hofmann, A.; Sauer, J. Ab Initio Study of Hydrogen Adsorption in MOF-5. *J. Am. Chem. Soc.* **2009**, *131*, 4143−4150.
(6) Dzubak, A. L.; Lin, L.-C.; Kim, J.; Swisher, J. A.; Poloni, R.; Maximoff, S. N.; Smit, B.; Gagliardi, L. Ab Initio Carbon Capture in Open-Site Metal−Organic Frameworks. *Nat. Chem.* **2012**, *4*, 810−816.
(7) Sladekova, K.; Campbell, C.; Grant, C.; Fletcher, A. J.; Gomes, J. R. B.; Jorge, M. The Effect of Atomic Point Charges On Adsorption Isotherms of CO_2 and Water in Metal Organic Frameworks. *Adsorption* **2020**, *26*, 663−685.
(8) Bureekaew, S.; Shimomura, S.; Kitagawa, S. Chemistry and Application of Flexible Porous Coordination Polymers. *Sci. Technol. Adv. Mater.* **2008**, *9*, No. 014108.
(9) Ferey, G.; Serre, C. Large Breathing Effects in Three-Dimensional Porous Hybrid Matter: Facts, Analyses, Rules and Consequences. *Chem. Soc. Rev.* **2009**, *38*, 1380−1399.
(10) Kitagawa, S.; Kitaura, R.; Noro, S. Functional Porous Coordination Polymers. *Angew. Chem., Int. Ed.* **2004**, *43*, 2334−2375.
(11) Serre, C.; Millange, F.; Thouvenot, C.; Nogues, M.; Marsolier, G.; Louer, D.; Ferey, G. Very Large Breathing Effect in the First Nanoporous Chromium(III)-Based Solids: MIL-53 or $Cr^{III}(OH)\bullet\{O_2C\text{-}C_6H_4\text{-}CO_2\}\bullet\{HO_2C\text{-}C_6H_4\text{-}CO_2H\}_x\bullet H_2O_y$. *J. Am. Chem. Soc.* **2002**, *124*, 13519−13526.
(12) Dissegna, S.; Epp, K.; Heinz, W. R.; Kieslich, G.; Fischer, R. A. Defective Metal-Organic Frameworks. *Adv. Mater.* **2018**, *30*, 1704501.
(13) Hou, J. W.; Sapnik, A. F.; Bennett, T. D. Metal-Organic Framework Gels and Monoliths. *Chem. Sci.* **2020**, *11*, 310−323.
(14) Oppenheim, J. J.; Skorupskii, G.; Dincă, M. Aperiodic Metal−Organic Frameworks. *Chem. Sci.* **2020**, *11*, 11094−111−3.
(15) Tuffnell, J. M.; Ashling, C. W.; Hou, J. W.; Li, S. C.; Longley, L.; Gomez, M. L. R.; Bennett, T. D. Novel Metal-Organic Framework Materials: Blends, Liquids, Glasses and Crystal-Glass Composites. *Chem. Commun.* **2019**, *55*, 8705−8715.
(16) Bennett, T. D.; Cheetham, A. K.; Fuchs, A. H.; Coudert, F.-X. Interplay Between Defects, Disorder and Flexibility in Metal-Organic Frameworks. *Nat. Chem.* **2017**, *9*, 11−16.
(17) Jawahery, S.; Simon, C. M.; Braun, E.; Witman, M.; Tiana, D.; Vlaisavljevich, B.; Smit, B. Adsorbate-induced lattice deformation in IRMOF-74 series. *Nat. Commun.* **2017**, *8*, 13945.
(18) Kanoo, P.; Matsuda, R.; Sato, H.; Li, L.; Hosono, N.; Kitagawa, S. Pseudo-Gated Adsorption with Negligible Volume Change Evoked by Halogen-Bond Interaction in the Nanospace of MOFs. *Chem. - Eur. J.* **2020**, *26*, 2148−2153.
(19) Kapelewski, M. T.; Geier, S. J.; Hudson, M. R.; Stück, D.; Mason, J. A.; Nelson, J. N.; Xiao, D. J.; Hulvey, Z.; Gilmour, E.; FitzGerald, S. A.; Head-Gordon, M.; Brown, C. M.; Long, J. R. M_2(m-dobdc) (M = Mg, Mn, Fe, Co, Ni) Metal−Organic Frameworks Exhibiting Increased Charge Density and Enhanced H_2 Binding at the Open Metal Sites. *J. Am. Chem. Soc.* **2014**, *136*, 12119−12129.
(20) Witman, M.; Ling, S.; Jawahery, S.; Boyd, P. G.; Haranczyk, M.; Slater, B.; Smit, B. The Influence of Intrinsic Framework Flexibility on Adsorption in Nanoporous Materials. *J. Am. Chem. Soc.* **2017**, *139*, 5547−5557.
(21) Witman, M.; Wright, B.; Smit, B. Simulating Enhanced Methane Deliverable Capacity of Guest Responsive Pores in Intrinsically Flexible MOFs. *J. Phys. Chem. Lett.* **2019**, *10*, 5929−5934.
(22) Gonzalez, M. I.; Kapelewski, M. T.; Bloch, E. D.; Milner, P. J.; Reed, D. A.; Hudson, M. R.; Mason, J. A.; Barin, G.; Brown, C. M.; Long, J. R. Separation of Xylene Isomers through Multiple Metal Site Interactions in Metal−Organic Frameworks. *J. Am. Chem. Soc.* **2018**, *140*, 3412−3422.
(23) McDonald, T. M.; Mason, J. A.; Kong, X.; Bloch, E. D.; Gygi, D.; Dani, A.; Crocellà, V.; Giordanino, F.; Odoh, S. O.; Drisdell, W. S.; Vlaisavljevich, B.; Dzubak, A. L.; Poloni, R.; Schnell, S. K.; Planas, N.; Lee, K.; Pascal, T.; Wan, L. F.; Prendergast, D.; Neaton, J. B.; Smit, B.; Kortright, J. B.; Gagliardi, L.; Bordiga, S.; Reimer, J. A.; Long, J. R. Cooperative Insertion of CO2 in Diamine-Appended Metal-Organic Frameworks. *Nature* **2015**, *519*, 303−308.
(24) Milner, P. J.; Martell, J. D.; Siegelman, R. L.; Gygi, D.; Weston, S. C.; Long, J. R. Overcoming Double-Step CO_2 Adsorption and Minimizing Water Co-Adsorption in Bulky Diamine-Appended Variants of Mg_2(dobpdc). *Chem. Sci.* **2018**, *9*, 160−174.
(25) Stavila, V.; Foster, M. E.; Brown, J. W.; Davis, R. W.; Edgington, J.; Benin, A. I.; Zarkesh, R. A.; Parthasarathi, R.; Hoyt, D. W.; Walter, E. D.; Andersen, A.; Washton, N. M.; Lipton, A. S.; Allendorf, M. D. IRMOF-74(n)−Mg: a Novel Catalyst Series for Hydrogen Activation and Hydrogenolysis of C−O bonds. *Chem. Sci.* **2019**, *10*, 9880−9892.
(26) Schneider, C.; Ukaj, D.; Koerver, R.; Talin, A. A.; Kieslich, G.; Pujari, S. P.; Zuilhof, H.; Janek, J.; Allendorf, M. D.; Fischer, R. A. High Electrical Conductivity and High Porosity in a Guest@MOF Material: Evidence of TCNQ Ordering Within Cu_3BTC_2 Micropores. *Chem. Sci.* **2018**, *9*, 7405−7412.
(27) Talin, A. A.; Centrone, A.; Ford, A. C.; Foster, M. E.; Stavila, V.; Haney, P.; Kinney, R. A.; Szalai, V.; El Gabaly, F.; Yoon, H. P.; Leonard, F.; Allendorf, M. D. Tunable Electrical Conductivity in Metal-Organic Framework Thin-Film Devices. *Science* **2014**, *343*, 66−69.
(28) Dürholt, J. P.; Jahromi, B. F.; Schmid, R. Tuning the Electric Field Response of MOFs by Rotatable Dipolar Linkers. *ACS Cent. Sci.* **2019**, *5*, 1440−1448.
(29) Bauer, C. A.; Timofeeva, T. V.; Settersten, T. B.; Patterson, B. D.; Liu, V. H.; Simmons, B. A.; Allendorf, M. D. Influence of Connectivity and Porosity On Ligand-Based Luminescence in Zinc Metal-Organic Frameworks. *J. Am. Chem. Soc.* **2007**, *129*, 7136−7144.
(30) Douvali, A.; Tsipis, A. C.; Eliseeva, S. V.; Petoud, S.; Papaefstathiou, G. S.; Malliakas, C. D.; Papadas, I.; Armatas, G. S.; Margiolaki, I.; Kanatzidis, M. G.; Lazarides, T.; Manos, M. J. Turn-On Luminescence Sensing and Real-Time Detection of Traces of Water in Organic Solvents by a Flexible Metal-Organic Framework. *Angew. Chem., Int. Ed.* **2015**, *54*, 1651−1656.
(31) Maka, V. K.; Mukhopadhyay, A.; Savitha, G.; Moorthy, J. N. Fluorescent 2D Metal-Organic Framework Nanosheets (MONs): Design, Synthesis and Sensing of Explosive Nitroaromatic Compounds (NACs). *Nanoscale* **2018**, *10*, 22389−22399.
(32) Shustova, N. B.; McCarthy, B. D.; Dinca, M. Turn-On Fluorescence in Tetraphenylethylene-Based Metal-Organic Frameworks: An Alternative to Aggregation-Induced Emission. *J. Am. Chem. Soc.* **2011**, *133*, 20126−20129.
(33) Zhang, M.; Feng, G.; Song, Z.; Zhou, Y.-P.; Chao, H.-Y.; Yuan, D.; Tan, T. T. Y.; Guo, Z.; Hu, Z.; Tang, B. Z.; Liu, B.; Zhao, D. Two-Dimensional Metal−Organic Framework with Wide Channels and Responsive Turn-On Fluorescence for the Chemical Sensing of Volatile Organic Compounds. *J. Am. Chem. Soc.* **2014**, *136*, 7241−7244.
(34) Butler, K. T.; Hendon, C. H.; Walsh, A. Electronic Chemical Potentials of Porous Metal-Organic Frameworks. *J. Am. Chem. Soc.* **2014**, *136*, 2703−2706.
(35) Cmarik, G. E.; Kim, M.; Cohen, S. M.; Walton, K. S. Tuning the Adsorption Properties of UiO-66 via Ligand Functionalization. *Langmuir* **2012**, *28*, 15606−15613.

https://doi.org/10.1021/jacs.0c10777
J. Am. Chem. Soc. XXXX, XXX, XXX−XXX

(36) Wiersum, A. D.; Soubeyrand-Lenoir, E.; Yang, Q.; Moulin, B.; Guillerm, V.; Yahia, M. B.; Bourrelly, S.; Vimont, A.; Miller, S.; Vagner, C.; Daturi, M.; Clet, G.; Serre, C.; Maurin, G.; Llewellyn, P. L. An Evaluation of UiO-66 for Gas-Based Applications. *Chem. - Asian J.* **2011**, *6*, 3270−3280.
(37) Chui, S. S.-Y.; Lo, S. M.-F.; Charmant, J. P. H.; Orpen, A. G.; Williams, I. D. A Chemically Functionalizable Nanoporous Material $[Cu_3(TMA)_2(H_2O)_3]_n$. *Science* **1999**, *283*, 1148−1150.
(38) Perry, J. J.; Teich-McGoldrick, S. L.; Meek, S. T.; Greathouse, J. A.; Haranczyk, M.; Allendorf, M. D. Noble Gas Adsorption in Metal−Organic Frameworks Containing Open Metal Sites. *J. Phys. Chem. C* **2014**, *118*, 11685−11698.
(39) Schneider, C. Retrofitting Metal-Organic Frameworks: TCNQ@Cu_3BTC_2 as a Case Study for Functional Material Design. Ph.D. Thesis, Technischen Universität München, 2019. https://mediatum.ub.tum.de/doc/1516469/1516469.pdf.
(40) Schneider, C.; Bodesheim, D.; Keupp, J.; Schmid, R.; Kieslich, G. Retrofitting metal-organic frameworks. *Nat. Commun.* **2019**, *10*, 4921.
(41) Lin, X.; Telepeni, I.; Blake, A. J.; Dailly, A.; Brown, C. M.; Simmons, J. M.; Zoppi, M.; Walker, G. S.; Thomas, K. M.; Mays, T. J.; Hubberstey, P.; Champness, N. R.; Schroder, M. High Capacity Hydrogen Adsorption in Cu(II) Tetracarboxylate Framework Materials: the Role of Pore Size, Ligand Functionalization, and Exposed Metal Sites. *J. Am. Chem. Soc.* **2009**, *131*, 2159−2171.
(42) Yan, Y.; Yang, S.; Blake, A. J.; Schröder, M. Studies on Metal−Organic Frameworks of Cu(II) with Isophthalate Linkers for Hydrogen Storage. *Acc. Chem. Res.* **2014**, *47*, 296−307.
(43) Ma, S. Q.; Sun, D. F.; Simmons, J. M.; Collier, C. D.; Yuan, D. Q.; Zhou, H. C. Metal-Organic Framework from An Anthracene Derivative Containing Nanoscopic Cages Exhibiting High Methane Uptake. *J. Am. Chem. Soc.* **2008**, *130*, 1012−1016.
(44) Heinke, L.; Wöll, C. Surface-Mounted Metal−Organic Frameworks: Crystalline and Porous Molecular Assemblies for Fundamental Insights and Advanced Applications. *Adv. Mater.* **2019**, *31*, 1806324.
(45) Stavila, V.; Schneider, C.; Mowry, C.; Zeitler, T. R.; Greathouse, J. A.; Robinson, A. L.; Denning, J. M.; Volponi, J.; Leong, K.; Quan, W.; Tu, M.; Fischer, R. A.; Allendorf, M. D. Thin Film Growth of nbo MOFs and Their Integration with Electroacoustic Devices. *Adv. Funct. Mater.* **2016**, *26*, 1699−1707.
(46) Stavila, V.; Volponi, J.; Katzenmeyer, A. M.; Dixon, M. C.; Allendorf, M. D. Kinetics and Mechanism of Metal-Organic Framework Thin Film Growth: Systematic Investigation of HKUST-1 Deposition on QCM Electrodes. *Chem. Sci.* **2012**, *3*, 1531−1540.
(47) Li, J.; Yu, X.; Xu, M.; Liu, W.; Sandraz, E.; Lan, H.; Wang, J.; Cohen, S. M. Metal−Organic Frameworks as Micromotors with Tunable Engines and Brakes. *J. Am. Chem. Soc.* **2017**, *139*, 611−614.
(48) Li, T.; Kozlowski, M. T.; Doud, E. A.; Blakely, M. N.; Rosi, N. L. Stepwise Ligand Exchange for the Preparation of a Family of Mesoporous MOFs. *J. Am. Chem. Soc.* **2013**, *135*, 11688−11691.
(49) Brozek, C. K.; Dincă, M. Ti^{3+}-, $V^{2+/3+}$-, $Cr^{2+/3+}$-, Mn^{2+}-, and Fe^{2+}-Substituted MOF-5 and Redox Reactivity in Cr- and Fe-MOF-5. *J. Am. Chem. Soc.* **2013**, *135*, 12886−12891.
(50) Dolgopolova, E. A.; Brandt, A. J.; Ejegbavwo, O. A.; Duke, A. S.; Maddumapatabandi, T. D.; Galhenage, R. P.; Larson, B. W.; Reid, O. G.; Ammal, S. C.; Heyden, A.; Chandrashekhar, M.; Stavila, V.; Chen, D. A.; Shustova, N. B. Electronic Properties of Bimetallic Metal−Organic Frameworks (MOFs): Tailoring the Density of Electronic States through MOF Modularity. *J. Am. Chem. Soc.* **2017**, *139*, 5201−5209.
(51) Kalmutzki, M. J.; Hanikel, N.; Yaghi, O. M. Secondary Building Units As the Turning Point in the Development of the Reticular Chemistry of MOFs. *Sci. Adv.* **2018**, *4*, No. eaat9180.
(52) Yuan, S.; Qin, J.-S.; Zou, L.; Chen, Y.-P.; Wang, X.; Zhang, Q.; Zhou, H.-C. Thermodynamically Guided Synthesis of Mixed-Linker Zr-MOFs with Enhanced Tunability. *J. Am. Chem. Soc.* **2016**, *138*, 6636−6642.
(53) Cheetham, A. K.; Bennett, T. D.; Coudert, F.-X.; Goodwin, A. L. Defects and Disorder in Metal Organic Frameworks. *Dalton Trans.* **2016**, *45*, 4113−4126.
(54) Gruza, B.; Chodkiewicz, M. L.; Krzeszczakowska, J.; Dominiak, P. M. Refinement of Organic Crystal Structures With Multipolar Electron Scattering Factors. *Acta Crystallogr., Sect. A: Found. Adv.* **2020**, *76*, 92−109.
(55) Lee, S.; Bürgi, H.-B.; Alshmimri, S. A.; Yaghi, O. M. Impact of Disordered Guest−Framework Interactions on the Crystallography of Metal−Organic Frameworks. *J. Am. Chem. Soc.* **2018**, *140*, 8958−8964.
(56) Appelhans, L. N.; Kosa, M.; Radha, A. V.; Simoncic, P.; Navrotsky, A.; Parrinello, M.; Cheetham, A. K. Phase Selection and Energetics in Chiral Alkaline Earth Tartrates and Their Racemic and Meso Analogues: Synthetic, Structural, Computational, and Calorimetric Studies. *J. Am. Chem. Soc.* **2009**, *131*, 15375−15386.
(57) Deng, H.; Doonan, C. J.; Furukawa, H.; Ferreira, R. B.; Towne, J.; Knobler, C. B.; Wang, B.; Yaghi, O. M. Multiple Functional Groups of Varying Ratios in Metal-Organic Frameworks. *Science* **2010**, *327*, 846.
(58) Wang, L. J.; Deng, H.; Furukawa, H.; Gándara, F.; Cordova, K. E.; Peri, D.; Yaghi, O. M. Synthesis and Characterization of Metal−Organic Framework-74 Containing 2, 4, 6, 8, and 10 Different Metals. *Inorg. Chem.* **2014**, *53*, 5881−5883.
(59) Furukawa, H.; Müller, U.; Yaghi, O. M. Heterogeneity within Order" in Metal−Organic Frameworks. *Angew. Chem., Int. Ed.* **2015**, *54*, 3417−3430.
(60) Ji, Z.; Li, T.; Yaghi, O. M. Sequencing of Metals in Multivariate Metal-Organic Frameworks. *Science* **2020**, *369*, 674.
(61) Griffin, S. L.; Champness, N. R. A Periodic Table of Metal-Organic Frameworks. *Coord. Chem. Rev.* **2020**, *414*, 213295.
(62) Halder, A.; Ghoshal, D. Structure and Properties of Dynamic Metal-Organic Frameworks: a Brief Accounts of Crystalline-To-Crystalline and Crystalline-To-Amorphous Transformations. *CrystEngComm* **2018**, *20*, 1322−1345.
(63) Castillo-Blas, C.; Moreno, J. M.; Romero-Muñiz, I.; Platero-Prats, A. E. Applications of Pair Distribution Function Analyses to the Emerging Field of Non-Ideal Metal−Organic Framework Materials. *Nanoscale* **2020**, *12*, 15577−15587.
(64) Bordiga, S.; Bonino, F.; Lillerud, K. P.; Lamberti, C. X-ray absorption Spectroscopies: Useful Tools to Understand Metallorganic Frameworks Structure and Reactivity. *Chem. Soc. Rev.* **2010**, *39*, 4885−4927.
(65) Zhang, D.; Zhu, Y.; Liu, L.; Ying, X.; Hsiung, C.-E.; Sougrat, R.; Li, K.; Han, Y. Atomic-Resolution Transmission Electron Microscopy of Electron Beam−Sensitive Crystalline Materials. *Science* **2018**, *359*, 675.
(66) Liu, L.; Zhang, D.; Zhu, Y.; Han, Y. Bulk and Local Structures of Metal−Organic Frameworks Unravelled by High-Resolution Electron Microscopy. *Communications Chem.* **2020**, *3*, 2399−3669.
(67) Frahm, D.; Hoffmann, F.; Fröba, M. Two Metal−Organic Frameworks with a Tetratopic Linker: Solvent-Dependent Polymorphism and Postsynthetic Bromination. *Cryst. Growth Des.* **2014**, *14*, 1719−1725.
(68) Hendon, C. H.; Walsh, A.; Akiyama, N.; Konno, Y.; Kajiwara, T.; Ito, T.; Kitagawa, H.; Sakai, K. One-Dimensional Magnus-Type Platinum Double Salts. *Nat. Commun.* **2016**, *7*, 11950.
(69) Krause, S.; Bon, V.; Senkovska, I.; Stoeck, U.; Wallacher, D.; Többens, D. M.; Zander, S.; Pillai, R. S.; Maurin, G.; Coudert, F.-X.; Kaskel, S. A Pressure-Amplifying Framework Material With Negative Gas Adsorption Transitions. *Nature* **2016**, *532*, 348−352.
(70) Lee, S.-J.; Mancuso, J. L.; Le, K. N.; Malliakas, C. D.; Bae, Y.-S.; Hendon, C. H.; Islamoglu, T.; Farha, O. K. Time-Resolved in Situ Polymorphic Transformation from One 12-Connected Zr-MOF to Another. *ACS Mater. Lett.* **2020**, *2*, 499−504.
(71) Akimbekov, Z.; Katsenis, A. D.; Nagabhushana, G. P.; Ayoub, G.; Arhangelskis, M.; Morris, A. J.; Friščić, T.; Navrotsky, A. Experimental and Theoretical Evaluation of the Stability of True MOF Polymorphs Explains Their Mechanochemical Interconversions. *J. Am. Chem. Soc.* **2017**, *139*, 7952−7957.
(72) Katsenis, A. D.; Puškarić, A.; Štrukil, V.; Mottillo, C.; Julien, P. A.; Užarević, K.; Pham, M. H.; Do, T. O.; Kimber, S. A.; Lazić, P.; Magdysyuk, O.; Dinnebier, R. E.; Halasz, I.; Friščić, T. in Situ X-Ray Diffraction Monitoring of a Mechanochemical Reaction Reveals a

https://doi.org/10.1021/jacs.0c10777
J. Am. Chem. Soc. XXXX, XXX, XXX−XXX

Unique Topology Metal-Organic Framework. *Nat. Commun.* **2015**, *6*, 6662.
(73) Gaillac, R.; Pullumbi, P.; Beyer, K. A.; Chapman, K. W.; Keen, D. A.; Bennett, T. D.; Coudert, F.-X. Liquid Metal−Organic Frameworks. *Nat. Mater.* **2017**, *16*, 1149−1154.
(74) Planas, N.; Mondloch, J. E.; Tussupbayev, S.; Borycz, J.; Gagliardi, L.; Hupp, J. T.; Farha, O. K.; Cramer, C. J. Defining the Proton Topology of the Zr6-Based Metal−Organic Framework NU-1000. *J. Phys. Chem. Lett.* **2014**, *5*, 3716−3723.
(75) Brozek, C. K.; Michaelis, V. K.; Ong, T.-C.; Bellarosa, L.; López, N.; Griffin, R. G.; Dincă, M. Dynamic DMF Binding in MOF-5 Enables the Formation of Metastable Cobalt-Substituted MOF-5 Analogues. *ACS Cent. Sci.* **2015**, *1*, 252−260.
(76) Brozek, C. K.; Ozarowski, A.; Stoian, S. A.; Dincă, M. Dynamic Structural Flexibility of Fe-MOF-5 Evidenced by 57Fe Mössbauer Spectroscopy. *Inorg. Chem. Front.* **2017**, *4*, 782−788.
(77) Lo, S.-H.; Feng, L.; Tan, K.; Huang, Z.; Yuan, S.; Wang, K.-Y.; Li, B.-H.; Liu, W.-L.; Day, G. S.; Tao, S.; Yang, C.-C.; Luo, T.-T.; Lin, C.-H.; Wang, S.-L.; Billinge, S. J. L.; Lu, K.-L.; Chabal, Y. J.; Zou, X.; Zhou, H.-C. Rapid Desolvation-Triggered Domino Lattice Rearrangement in a Metal−Organic Framework. *Nat. Chem.* **2020**, *12*, 90−97.
(78) Brozek, C. K.; Dincă, M. Cation Exchange At the Secondary Building Units of Metal−Organic Frameworks. *Chem. Soc. Rev.* **2014**, *43*, 5456−5467.
(79) Brozek, C. K.; Dincă, M. Thermodynamic Parameters of Cation Exchange in MOF-5 and MFU-4l. *Chem. Commun.* **2015**, *51*, 11780−11782.
(80) Brozek, C. K.; Bellarosa, L.; Soejima, T.; Clark, T. V.; López, N.; Dincă, M. Solvent-Dependent Cation Exchange in Metal−Organic Frameworks. *Chem. - Eur. J.* **2014**, *20*, 6871−6874.
(81) Kim, M.; Cahill, J. F.; Su, Y.; Prather, K. A.; Cohen, S. M. Postsynthetic Ligand Exchange As a Route to Functionalization of 'Inert' Metal−Organic Frameworks. *Chem. Sci.* **2012**, *3*, 126−130.
(82) Marreiros, J.; Caratelli, C.; Hajek, J.; Krajnc, A.; Fleury, G.; Bueken, B.; De Vos, D. E.; Mali, G.; Roeffaers, M. B. J.; Van Speybroeck, V.; Ameloot, R. Active Role of Methanol in Post-Synthetic Linker Exchange in the Metal−Organic Framework UiO-66. *Chem. Mater.* **2019**, *31*, 1359−1369.
(83) Zhou, W.; Wu, H.; Yildirim, T.; Simpson, J. R.; Walker, A. R. H. Origin of the Exceptional Negative Thermal Expansion in Metal-Organic Framework-5 Zn_4O (1,4-benzenedicarboxylate)$_3$. *Phys. Rev. B: Condens. Matter Mater. Phys.* **2008**, *78*, No. 054114.
(84) Wu, Y.; Kobayashi, A.; Halder, G. J.; Peterson, V. K.; Chapman, K. W.; Lock, N.; Southon, P. D.; Kepert, C. J. Negative Thermal Expansion in the Metal−Organic Framework Material Cu_3(1,3,5-benzenetricarboxylate)$_2$. *Angew. Chem., Int. Ed.* **2008**, *47*, 8929−8932.
(85) Schneider, C.; Bodesheim, D.; Ehrenreich, M. G.; Crocellà, V.; Mink, J.; Fischer, R. A.; Butler, K. T.; Kieslich, G. Tuning the Negative Thermal Expansion Behavior of the Metal−Organic Framework Cu_3BTC_2 by Retrofitting. *J. Am. Chem. Soc.* **2019**, *141*, 10504−10509.
(86) Lock, N.; Christensen, M.; Kepert, C. J.; Iversen, B. B. Effect of Gas Pressure on Negative Thermal Expansion in MOF-5. *Chem. Commun.* **2013**, *49*, 789−791.
(87) Balestra, S. R. G.; Bueno-Perez, R.; Hamad, S.; Dubbeldam, D.; Ruiz-Salvador, A. R.; Calero, S. Controlling Thermal Expansion: a Metal−Organic Frameworks Route. *Chem. Mater.* **2016**, *28*, 8296−8304.
(88) Babaei, H.; DeCoster, M. E.; Jeong, M.; Hassan, Z. M.; Islamoglu, T.; Baumgart, H.; McGaughey, A. J. H.; Redel, E.; Farha, O. K.; Hopkins, P. E.; Malen, J. A.; Wilmer, C. E. Observation of Reduced Thermal Conductivity in a Metal-Organic Framework Due to the Presence of Adsorbates. *Nat. Commun.* **2020**, *11*, 4010.
(89) Babaei, H.; McGaughey, A. J. H.; Wilmer, C. E. Effect of Pore Size and Shape on the Thermal Conductivity of Metal-Organic Frameworks. *Chem. Sci.* **2017**, *8*, 583−589.
(90) Meilikhov, M.; Yusenko, K.; Fischer, R. A. Incorporation of Metallocenes Into the Channel Structured Metal-Organic Frameworks MIL-53(Al) and MIL-47(V). *Dalton Trans.* **2010**, *39*, 10990−10999.
(91) Thürmer, K.; Schneider, C.; Stavila, V.; Friddle, R. W.; Léonard, F.; Fischer, R. A.; Allendorf, M. D.; Talin, A. A. Surface Morphology and Electrical Properties of Cu_3BTC_2 Thin Films Before and After Reaction with TCNQ. *ACS Appl. Mater. Interfaces* **2018**, *10*, 39400−39410.
(92) Heintz, R. A.; Zhao, H.; Ouyang, X.; Grandinetti, G.; Cowen, J.; Dunbar, K. R. New Insight Into the Nature of Cu(TCNQ): Solution Routes to Two Distinct Polymorphs and Their Relationship to Crystalline Films That Display Bistable Switching Behavior. *Inorg. Chem.* **1999**, *38*, 144−156.
(93) Schneider, C.; Mendt, M.; Poppl, A.; Crocella, V.; Fischer, R. A. Scrutinizing the Pore Chemistry and the Importance of Cu(I) Defects in TCNQ-Loaded $Cu_3(BTC)_2$ by a Multitechnique Spectroscopic Approach. *ACS Appl. Mater. Interfaces* **2020**, *12*, 1024−1035.
(94) D'Alessandro, D. M.; Kanga, J. R. R.; Caddy, J. S. Towards Conducting Metal-Organic Frameworks. *Aust. J. Chem.* **2011**, *64*, 718−722.
(95) Calbo, J.; Golomb, M. J.; Walsh, A. Redox-Active Metal−Organic Frameworks for Energy Conversion and Storage. *J. Mater. Chem. A* **2019**, *7*, 16571−16597.
(96) Nijem, N.; Bluhm, H.; Ng, M. L.; Kunz, M.; Leone, S. R.; Gilles, M. K. Cu^{1+} in HKUST-1: Selective Gas Adsorption in the Presence of Water. *Chem. Commun.* **2014**, *50*, 10144−10147.
(97) Prestipino, C.; Regli, L.; Vitillo, J. G.; Bonino, F.; Damin, A.; Lamberti, C.; Zecchina, A.; Solari, P. L.; Kongshaug, K. O.; Bordiga, S. Local Structure of Framework Cu(II) in HKUST-1 Metallorganic Framework: Spectroscopic Characterization Upon Activation and Interaction With Adsorbates. *Chem. Mater.* **2006**, *18*, 1337−1346.
(98) Todaro, M.; Buscarino, G.; Sciortino, L.; Alessi, A.; Messina, F.; Taddei, M.; Ranocchiari, M.; Cannas, M.; Gelardi, F. M. Decomposition Process of Carboxylate MOF HKUST-1 Unveiled at the Atomic Scale Level. *J. Phys. Chem. C* **2016**, *120*, 12879−12889.
(99) Bordiga, S.; Regli, L.; Bonino, F.; Groppo, E.; Lamberti, C.; Xiao, B.; Wheatley, P. S.; Morris, R. E.; Zecchina, A. Adsorption Properties of HKUST-1 Toward Hydrogen and Other Small Molecules Monitored by IR. *Phys. Chem. Chem. Phys.* **2007**, *9*, 2676−2685.
(100) Drenchev, N.; Rosnes, M. H.; Dietzel, P. D. C.; Albinati, A.; Hadjiivanov, K.; Georgiev, P. A. Open Metal Sites in the Metal-Organic Framework CPO-27-Cu: Detection of Regular and Defect Copper Species by CO and NO Probe Molecules. *J. Phys. Chem. C* **2018**, *122*, 17238−17249.
(101) Szanyi, J.; Daturi, M.; Clet, G.; Baer, D. R.; Peden, C. H. F. Well-studied Cu−BTC Still Serves Surprises: Evidence for Facile Cu2+/Cu+ Interchange. *Phys. Chem. Chem. Phys.* **2012**, *14*, 4383−4390.
(102) St. Petkov, P.; Vayssilov, G. N.; Liu, J.; Shekhah, O.; Wang, Y.; Wöll, C.; Heine, T. Defects in MOFs: a Thorough Characterization. *ChemPhysChem* **2012**, *13*, 2025−2029.
(103) Yang, J.; Regier, T.; Dynes, J. J.; Wang, J.; Shi, J.; Peak, D.; Zhao, Y.; Hu, T.; Chen, Y.; Tse, J. S. Soft X-ray Induced Photoreduction of Organic Cu(II) Compounds Probed by X-ray Absorption Near-Edge (XANES) Spectroscopy. *Anal. Chem.* **2011**, *83*, 7856−7862.
(104) Zhang, W. H.; Kauer, M.; Guo, P. H.; Kunze, S.; Cwik, S.; Muhler, M.; Wang, Y. M.; Epp, K.; Kieslich, G.; Fischer, R. A. Impact of Synthesis Parameters on the Formation of Defects in HKUST-1. *Eur. J. Inorg. Chem.* **2017**, *2017*, 925−931.
(105) Müller, K.; Fink, K.; Schöttner, L.; Koenig, M.; Heinke, L.; Wöll, C. Defects as Color Centers: the Apparent Color of Metal−Organic Frameworks Containing Cu^{2+}-Based Paddle-Wheel Units. *ACS Appl. Mater. Interfaces* **2017**, *9*, 37463−37467.
(106) Simenas, M.; Kobalz, M.; Mendt, M.; Eckold, P.; Krautscheid, H.; Banys, J.; Poppl, A. Synthesis, Structure, and Electron Paramagnetic Resonance Study of a Mixed Valent Metal-Organic Framework Containing Cu_2 Paddle-Wheel Units. *J. Phys. Chem. C* **2015**, *119*, 4898−4907.
(107) Park, J. G.; Aubrey, M. L.; Oktawiec, J.; Chakarawet, K.; Darago, L. E.; Grandjean, F.; Long, G. J.; Long, J. R. Charge Delocalization and Bulk Electronic Conductivity in the Mixed-Valence Metal−Organic Framework Fe(1,2,3-triazolate)$_2$(BF_4)$_x$. *J. Am. Chem. Soc.* **2018**, *140*, 8526−8534.

https://doi.org/10.1021/jacs.0c10777
J. Am. Chem. Soc. XXXX, XXX, XXX−XXX

(108) Gandara, F.; Uribe-Romo, F. J.; Britt, D. K.; Furukawa, H.; Lei, L.; Cheng, R.; Duan, X.; O'Keeffe, M.; Yaghi, O. M. Porous, Conductive Metal-Triazolates and Their Structural Elucidation by the Charge-Flipping Method. *Chem. - Eur. J.* **2012**, *18*, 10595−10601.
(109) Day, R. W.; Bediako, D. K.; Rezaee, M.; Parent, L. R.; Skorupskii, G.; Arguilla, M. Q.; Hendon, C. H.; Stassen, I.; Gianneschi, N. C.; Kim, P.; Dincă, M. Single Crystals of Electrically Conductive Two-Dimensional Metal−Organic Frameworks: Structural and Electrical Transport Properties. *ACS Cent. Sci.* **2019**, *5*, 1959−1964.
(110) Dou, J.-H.; Arguilla, M. Q.; Luo, Y.; Li, J.; Zhang, W.; Sun, L.; Mancuso, J. L.; Yang, L.; Chen, T.; Parent, L. R.; Skorupskii, G.; Libretto, N. J.; Sun, C.; Yang, M. C.; Dip, P. V.; Brignole, E. J.; Miller, J. T.; Kong, J.; Hendon, C. H.; Sun, J.; Dincă, M. Atomically Precise Single-Crystal Structures of Electrically Conducting 2D Metal−Organic Frameworks. *Nat. Mater.* **2021**, *20*, 222−228.
(111) Skorupskii, G.; Trump, B. A.; Kasel, T. W.; Brown, C. M.; Hendon, C. H.; Dincă, M. Efficient and Tunable One-Dimensional Charge Transport in Layered Lanthanide Metal−Organic Frameworks. *Nat. Chem.* **2020**, *12*, 131−136.
(112) Sheberla, D.; Sun, L.; Blood-Forsythe, M. A.; Er, S.; Wade, C. R.; Brozek, C. K.; Aspuru-Guzik, A.; Dinca, M. High Electrical Conductivity in Ni_3(2,3,6,7,10,11-hexaiminotriphenylene)$_2$, a Semiconducting Metal-Organic Graphene Analogue. *J. Am. Chem. Soc.* **2014**, *136*, 8859−8862.
(113) Foster, M. E.; Sohlberg, K.; Allendorf, M. D.; Talin, A. A. Unraveling the Semiconducting/Metallic Discrepancy in $Ni_3(HITP)_2$. *J. Phys. Chem. Lett.* **2018**, *9*, 481−486.
(114) Rogge, S. M. J.; Goeminne, R.; Demuynck, R.; Gutierrez-Sevillano, J. J.; Vandenbrande, S.; Vanduyfhuys, L.; Waroquier, M.; Verstraelen, T.; Van Speybroeck, V. Modeling Gas Adsorption in Flexible Metal−Organic Frameworks via Hybrid Monte Carlo/Molecular Dynamics Schemes. *Adv. Theory Simul.* **2019**, *2*, 1800177.
(115) Henke, S.; Fischer, R. A. Gated Channels in a Honeycomb-like Zinc−Dicarboxylate−Bipyridine Framework with Flexible Alkyl Ether Side Chains. *J. Am. Chem. Soc.* **2011**, *133*, 2064−2067.
(116) He, J.; Yee, K.-K.; Xu, Z.; Zeller, M.; Hunter, A. D.; Chui, S. S.-Y.; Che, C.-M. Thioether Side Chains Improve the Stability, Fluorescence, and Metal Uptake of a Metal−Organic Framework. *Chem. Mater.* **2011**, *23*, 2940−2947.
(117) Halter, D. P.; Klein, R. A.; Boreen, M. A.; Trump, B. A.; Brown, C. M.; Long, J. R. Self-Adjusting Binding Pockets Enhance H_2 and CH_4 Adsorption in a Uranium-Based Metal − Organic Framework. *Chem. Sci.* **2020**, *11*, 6709−6716.
(118) Kapelewski, M. T.; Runčevski, T.; Tarver, J. D.; Jiang, H. Z. H.; Hurst, K. E.; Parilla, P. A.; Ayala, A.; Gennett, T.; FitzGerald, S. A.; Brown, C. M.; Long, J. R. Record High Hydrogen Storage Capacity in the Metal−Organic Framework Ni_2(m-dobdc) at Near-Ambient Temperatures. *Chem. Mater.* **2018**, *30*, 8179−8189.
(119) Rosen, A. S.; Mian, M. R.; Islamoglu, T.; Chen, H.; Farha, O. K.; Notestein, J. M.; Snurr, R. Q. Tuning the Redox Activity of Metal−Organic Frameworks for Enhanced, Selective O_2 Binding: Design Rules and Ambient Temperature O_2 Chemisorption in a Cobalt−Triazolate Framework. *J. Am. Chem. Soc.* **2020**, *142*, 4317−4328.
(120) Deng, H.; Grunder, S.; Cordova, K. E.; Valente, C.; Furukawa, H.; Hmadeh, M.; Gándara, F.; Whalley, A. C.; Liu, Z.; Asahina, S.; Kazumori, H.; O'Keeffe, M.; Terasaki, O.; Stoddart, J. F.; Yaghi, O. M. Large-Pore Apertures in a Series of Metal-Organic Frameworks. *Science* **2012**, *336*, 1018−1023.
(121) Sung Cho, H.; Deng, H.; Miyasaka, K.; Dong, Z.; Cho, M.; Neimark, A. V.; Ku Kang, J.; Yaghi, O. M.; Terasaki, O. Extra Adsorption and Adsorbate Superlattice Formation in Metal-Organic Frameworks. *Nature* **2015**, *527*, 503−507.
(122) Li, H.; Wang, K.; Sun, Y.; Lollar, C. T.; Li, J.; Zhou, H.-C. Recent Advances in Gas Storage and Separation Using Metal−Organic Frameworks. *Mater. Today* **2018**, *21*, 108−121.
(123) Redfern, L. R.; Robison, L.; Wasson, M. C.; Goswami, S.; Lyu, J.; Islamoglu, T.; Chapman, K. W.; Farha, O. K. Porosity Dependence of Compression and Lattice Rigidity in Metal−Organic Framework Series. *J. Am. Chem. Soc.* **2019**, *141*, 4365−4371.
(124) Banerjee, D.; Simon, C. M.; Plonka, A. M.; Motkuri, R. K.; Liu, J.; Chen, X.; Smit, B.; Parise, J. B.; Haranczyk, M.; Thallapally, P. K. Metal−Organic Framework With Optimally Selective Xenon Adsorption and Separation. *Nat. Commun.* **2016**, *7*, 11831.
(125) McDonald, T. M.; Mason, J. A.; Kong, X.; Bloch, E. D.; Gygi, D.; Dani, A.; et al. Cooperative Insertion of CO_2 in Diamine-Appended Metal-Organic Frameworks. *Nature* **2015**, *519*, 303−308.
(126) Leus, K.; Muylaert, I.; Vandichel, M.; Marin, G. B.; Waroquier, M.; Van Speybroeck, V.; Van Der Voort, P. The Remarkable Catalytic Activity of the Saturated Metal Organic Framework V-MIL-47 in the Cyclohexene Oxidation. *Chem. Commun.* **2010**, *46*, 5085−5087.
(127) Leus, K.; Vandichel, M.; Liu, Y. Y.; Muylaert, I.; Musschoot, J.; Pyl, S.; Vrielinck, H.; Callens, F.; Marin, G. B.; Detavernier, C.; Wiper, P. V.; Khimyak, Y. Z.; Waroquier, M.; Van Speybroeck, V.; Van der Voort, P. The Coordinatively Saturated Vanadium MIL-47 as a Low Leaching Heterogeneous Catalyst in the Oxidation of Cyclohexene. *J. Catal.* **2012**, *285*, 196−207.
(128) Metzger, E. D.; Brozek, C. K.; Comito, R. J.; Dincă, M. Selective Dimerization of Ethylene to 1-Butene with a Porous Catalyst. *ACS Cent. Sci.* **2016**, *2*, 148−153.
(129) Metzger, E. D.; Comito, R. J.; Hendon, C. H.; Dincă, M. Mechanism of Single-Site Molecule-Like Catalytic Ethylene Dimerization in Ni-MFU-4l. *J. Am. Chem. Soc.* **2017**, *139*, 757−762.
(130) Bien, C. E.; Chen, K. K.; Chien, S.-C.; Reiner, B. R.; Lin, L.-C.; Wade, C. R.; Ho, W. S. W. Bioinspired Metal−Organic Framework for Trace CO_2 Capture. *J. Am. Chem. Soc.* **2018**, *140*, 12662−12666.
(131) Metzger, E. D.; Comito, R. J.; Wu, Z.; Zhang, G.; Dubey, R. C.; Xu, W.; Miller, J. T.; Dincă, M. Highly Selective Heterogeneous Ethylene Dimerization with a Scalable and Chemically Robust MOF Catalyst. *ACS Sustainable Chem. Eng.* **2019**, *7*, 6654−6661.
(132) Comito, R. J.; Fritzsching, K. J.; Sundell, B. J.; Schmidt-Rohr, K.; Dincă, M. Single-Site Heterogeneous Catalysts for Olefin Polymerization Enabled by Cation Exchange in a Metal-Organic Framework. *J. Am. Chem. Soc.* **2016**, *138*, 10232−10237.
(133) Comito, R. J.; Wu, Z.; Zhang, G.; Lawrence, J. A., III; Korzyński, M. D.; Kehl, J. A.; Miller, J. T.; Dincă, M. Stabilized Vanadium Catalyst for Olefin Polymerization by Site Isolation in a Metal−Organic Framework. *Angew. Chem., Int. Ed.* **2018**, *57*, 8135−8139.
(134) Sun, L.; Campbell, M. G.; Dinca, M. Electrically Conductive Porous Metal-Organic Frameworks. *Angew. Chem., Int. Ed.* **2016**, *55*, 3566−3579.
(135) Xie, L. S.; Skorupskii, G.; Dincă, M. Electrically Conductive Metal−Organic Frameworks. *Chem. Rev.* **2020**, *120*, 8536−8580.
(136) Shimomura, S.; Kitagawa, S. Soft Porous Crystal Meets TCNQ: Charge Transfer-Type Porous Coordination Polymers. *J. Mater. Chem.* **2011**, *21*, 5537−5546.
(137) Avendano, C.; Zhang, Z. Y.; Ota, A.; Zhao, H. H.; Dunbar, K. R. Dramatically Different Conductivity Properties of Metal-Organic Framework Polymorphs of Tl(TCNQ): An Unexpected Room-Temperature Crystal-to-Crystal Phase Transition. *Angew. Chem., Int. Ed.* **2011**, *50*, 6543−6547.
(138) Usman, M.; Mendiratta, S.; Lu, K. L. Semiconductor Metal-Organic Frameworks: Future Low-Bandgap Materials. *Adv. Mater.* **2017**, *29*, 1605071.
(139) Ling, S. L.; Slater, B. Unusually Large Band Gap Changes in Breathing Metal-Organic Framework Materials. *J. Phys. Chem. C* **2015**, *119*, 16667−16677.
(140) Gu, Z. G.; Heinke, L.; Woll, C.; Neumann, T.; Wenzel, W.; Li, Q.; Fink, K.; Gordan, O. D.; Zahn, D. R. T. Experimental and Theoretical Investigations of the Electronic Band Structure of Metal-Organic Frameworks of HKUST-1 Type. *Appl. Phys. Lett.* **2015**, *107*, 183301.
(141) Kapustin, E. A.; Lee, S.; Alshammari, A. S.; Yaghi, O. M. Molecular Retrofitting Adapts a Metal−Organic Framework to Extreme Pressure. *ACS Cent. Sci.* **2017**, *3*, 662−667.
(142) Allendorf, M. D.; Dong, R. H.; Feng, X. L.; Kaskel, S.; Matoga, D.; Stavila, V. Electronic Devices Using Open Framework Materials. *Chem. Rev.* **2020**, *120*, 8581−8640.

https://doi.org/10.1021/jacs.0c10777
J. Am. Chem. Soc. XXXX, XXX, XXX−XXX

(143) Stassen, I.; Dou, J.-H.; Hendon, C.; Dincă, M. Chemiresistive Sensing of Ambient CO_2 by an Autogenously Hydrated Cu_3(hexaiminobenzene)$_2$ Framework. *ACS Cent. Sci.* **2019**, *5*, 1425−1431.
(144) Perry, J. J.; Feng, P. L.; Meek, S. T.; Leong, K.; Doty, F. P.; Allendorf, M. D. Connecting structure with function in metal-organic frameworks to design novel photo- and radioluminescent materials. *J. Mater. Chem.* **2012**, *22*, 10235−10248.
(145) Cui, Y.; Yue, Y.; Qian, G.; Chen, B. Luminescent Functional Metal−Organic Frameworks. *Chem. Rev.* **2012**, *112*, 1126−1162.
(146) Gole, B.; Bar, A. K.; Mukherjee, P. S. Fluorescent Metal−Organic Framework for Selective Sensing of Nitroaromatic Explosives. *Chem. Commun.* **2011**, *47*, 12137−12139.
(147) Nagarkar, S. S.; Desai, A. V.; Ghosh, S. K. A Fluorescent Metal−Organic Framework for Highly Selective Detection of Nitro Explosives in the Aqueous Phase. *Chem. Commun.* **2014**, *50*, 8915−8918.
(148) Liu, G.-l.; Qin, Y.-j.; Jing, L.; Wei, G.-y.; Li, H. Two Novel MOF-74 Analogs Exhibiting Unique Luminescent Selectivity. *Chem. Commun.* **2013**, *49*, 1699−1701.
(149) Wu, Z.-F.; Tan, B.; Feng, M.-L.; Lan, A.-J.; Huang, X.-Y. A Magnesium MOF as a Sensitive Fluorescence Sensor for CS_2 and Nitroaromatic Compounds. *J. Mater. Chem. A* **2014**, *2*, 6426−6431.
(150) Wei, Z.; Gu, Z.-Y.; Arvapally, R. K.; Chen, Y.-P.; McDougald, R. N.; Ivy, J. F.; Yakovenko, A. A.; Feng, D.; Omary, M. A.; Zhou, H.-C. Rigidifying Fluorescent Linkers by Metal−Organic Framework Formation for Fluorescence Blue Shift and Quantum Yield Enhancement. *J. Am. Chem. Soc.* **2014**, *136*, 8269−8276.
(151) Mieno, H.; Kabe, R.; Notsuka, N.; Allendorf, M. D.; Adachi, C. Long-Lived Room-Temperature Phosphorescence of Coronene in Zeolitic Imidazolate Framework ZIF-8. *Adv. Opt. Mater.* **2016**, *4*, 1015−1021.
(152) Karmakar, A.; Samanta, P.; Dutta, S.; Ghosh, S. K. Fluorescent "Turn-on" Sensing Based on Metal−Organic Frameworks (MOFs). *Chem. - Asian J.* **2019**, *14*, 4506−4519.
(153) Yao, S.-L.; Liu, S.-J.; Tian, X.-M.; Zheng, T.-F.; Cao, C.; Niu, C.-Y.; Chen, Y.-Q.; Chen, J.-L.; Huang, H.; Wen, H.-R. A ZnII-Based Metal−Organic Framework with a Rare tcj Topology as a Turn-On Fluorescent Sensor for Acetylacetone. *Inorg. Chem.* **2019**, *58*, 3578−3581.
(154) Das, A.; Anbu, N.; Sk, M.; Dhakshinamoorthy, A.; Biswas, S. A Functionalized Uio-66 MOF for Turn-On Fluorescence Sensing of Superoxide in Water and Efficient Catalysis for Knoevenagel Condensation. *Dalton Trans.* **2019**, *48*, 17371−17380.
(155) Gui, B.; Meng, Y.; Xie, Y.; Tian, J.; Yu, G.; Zeng, W.; Zhang, G.; Gong, S.; Yang, C.; Zhang, D.; Wang, C. Tuning the Photoinduced Electron Transfer in a Zr-MOF: Toward Solid-State Fluorescent Molecular Switch and Turn-On Sensor. *Adv. Mater.* **2018**, *30*, 1802329.
(156) Jiang, H.-L.; Feng, D.; Wang, K.; Gu, Z.-Y.; Wei, Z.; Chen, Y.-P.; Zhou, H.-C. An Exceptionally Stable, Porphyrinic Zr Metal−Organic Framework Exhibiting pH-Dependent Fluorescence. *J. Am. Chem. Soc.* **2013**, *135*, 13934−13938.
(157) Witman, M.; Ling, S. L.; Stavila, V.; Wijeratne, P.; Furukawa, H.; Allendorf, M. D. Design Principles for the Ultimate Gas Deliverable Capacity Material: Nonporous to Porous Deformations Without Volume Change. *Mol. Sys. Des. Eng.* **2020**, *5*, 1491−1503.
(158) Ahmed, A.; Seth, S.; Purewal, J.; Wong-Foy, A. G.; Veenstra, M.; Matzger, A. J.; Siegel, D. J. Exceptional Hydrogen Storage Achieved by Screening Nearly Half a Million Metal-Organic Frameworks. *Nat. Commun.* **2019**, *10*, 1568.
(159) Moosavi, S. M.; Nandy, A.; Jablonka, K. M.; Ongari, D.; Janet, J. P.; Boyd, P. G.; Lee, Y.; Smit, B.; Kulik, H. J. Understanding the Diversity of the Metal-Organic Framework Ecosystem. *Nat. Commun.* **2020**, *11*, 4068.
(160) Mohamed, S. A.; Chong, S.; Kim, J. Thermal Stability of Methyl-Functionalized MOF-5. *J. Phys. Chem. C* **2019**, *123*, 29686−29692.
(161) Sanchez-Sanchez, M.; Getachew, N.; Diaz, K.; Diaz-Garcia, M.; Chebude, Y.; Diaz, I. Synthesis of Metal-Organic Frameworks in Water At Room Temperature: Salts As Linker Sources. *Green Chem.* **2015**, *17*, 1500−1509.
(162) Foster, M. E.; Sohlberg, K.; Spataru, C. D.; Allendorf, M. D. Proposed Modification of the Graphene Analogue Ni_3(HITP)$_2$ to Yield a Semiconducting Material. *J. Phys. Chem. C* **2016**, *120*, 15001−15008.
(163) Le, K. N.; Hendon, C. H. Pressure-Induced Metallicity and Piezoreductive Transition of Metal-Centres in Conductive 2-Dimensional Metal-Organic Frameworks. *Phys. Chem. Chem. Phys.* **2019**, *21*, 25773−25778.
(164) Butler, K. T.; Worrall, S. D.; Molloy, C. D.; Hendon, C. H.; Attfield, M. P.; Dryfe, R. A. W.; Walsh, A. Electronic Structure Design for Nanoporous, Electrically Conductive Zeolitic Imidazolate Frameworks. *J. Mater. Chem. C* **2017**, *5*, 7726−7731.
(165) Andreeva, A. B.; Le, K. N.; Chen, L. K.; Kellman, M. E.; Hendon, C. H.; Brozek, C. K. Soft Mode Metal-Linker Dynamics in Carboxylate MOFs Evidenced by Variable-Temperature Infrared Spectroscopy. *J. Am. Chem. Soc.* **2020**, *142*, 19291−19299.
(166) Baxter, S. J.; Schneemann, A.; Ready, A. D.; Wijeratne, P.; Wilkinson, A. P.; Burtch, N. C. Tuning Thermal Expansion in Metal-Organic Frameworks Using a Mixed Linker Solid Solution Approach. *J. Am. Chem. Soc.* **2019**, *141*, 12849−12854.
(167) Burtch, N. C.; Heinen, J.; Bennett, T. D.; Dubbeldam, D.; Allendorf, M. D. Mechanical Properties in Metal-Organic Frameworks: Emerging Opportunities and Challenges for Device Functionality and Technological Applications. *Adv. Mater.* **2018**, *30*, 1704124.
(168) Garai, B.; Bon, V.; Efimova, A.; Gerlach, M.; Senkovska, I.; Kaskel, S. Reversible Switching Between Positive and Negative Thermal Expansion in a Metal-Organic Framework DUT-49. *J. Mater. Chem. A* **2020**, *8*, 20420−20428.
(169) Gonzalez-Nelson, A.; Coudert, F. X.; van der Veen, M. A. Rotational Dynamics of Linkers in Metal-Organic Frameworks. *Nanomaterials* **2019**, *9*, 330.
(170) Allendorf, M. D.; Houk, R. J. T.; Andruszkiewicz, L.; Talin, A. A.; Pikarsky, J.; Choudhury, A.; Gall, K. A.; Hesketh, P. J. Stress-induced Chemical Detection Using Flexible Metal-Organic Frameworks. *J. Am. Chem. Soc.* **2008**, *130*, 14404−14405.
(171) Venkatasubramanian, A.; Lee, J. H.; Stavila, V.; Robinson, A.; Allendorf, M. D.; Hesketh, P. J. MOF@MEMS: Design Optimization for High Sensitivity Chemical Detection. *Sens. Actuators, B* **2012**, *168*, 256−262.
(172) Chen, D. S.; Xing, H. Z.; Su, Z. M.; Wang, C. G. Electrical Conductivity and Electroluminescence of a New Anthracene-Based Metal-Organic Framework With Pi-Conjugated Zigzag Chains. *Chem. Commun.* **2016**, *52*, 2019−2022.
(173) Gutierrez, M.; Martin, C.; Kennes, K.; Hofkens, J.; Vander Auweraer, M.; Sanchez, F.; Douhal, A. New OLEDs Based on Zirconium Metal-Organic Framework. *Adv. Opt. Mater.* **2018**, *6*, 1701060.
(174) Gutierrez, M.; Martin, C.; Van der Auweraer, M.; Hofkens, J.; Tan, J. C. Electroluminescent Guest@MOF Nanoparticles for Thin Film Optoelectronics and Solid-State Lighting. *Adv. Opt. Mater.* **2020**, *8*, 2000670.
(175) Haider, G.; Usman, M.; Chen, T. P.; Perumal, P.; Lu, K. L.; Chen, Y. F. Electrically Driven White Light Emission from Intrinsic Metal-Organic Framework. *ACS Nano* **2016**, *10*, 8366−8375.
(176) Haldar, R.; Jakoby, M.; Kozlowska, M.; Khan, M. R.; Chen, H. Y.; Pramudya, Y.; Richards, B. S.; Heinke, L.; Wenzel, W.; Odobel, F.; Diring, S.; Howard, I. A.; Lemmer, U.; Woll, C. Tuning Optical Properties by Controlled Aggregation: Electroluminescence Assisted by Thermally-Activated Delayed Fluorescence from Thin Films of Crystalline Chromophores. *Chem. - Eur. J.* **2020**, *26*, 17016−17020.
(177) Juang, F. S.; Yao, M. Q.; Mondal, T.; Saha, S. K. Electrically Driven MOF-Based Blue to Yellow-White Tunable Light Emitting Diodes. *IEEE Access* **2020**, *8*, 216986−216993.
(178) Ma, Y. N.; Cong, J. Z.; Chai, Y. S.; Yan, L. Q.; Shang, D. S.; Sun, Y. Large Pyroelectric and Thermal Expansion Coefficients in the $(CH_3)_2NH_2Mn(HCOO)_3$ Metal-Organic Framework. *Appl. Phys. Lett.* **2017**, *111*, No. 042901.
(179) Markey, K.; Putzeys, T.; Horcajada, P.; Devic, T.; Guillou, N.; Wubbenhorst, M.; Van Cleuvenbergen, S.; Verbiest, T.; De Vos, D. E.; van der Veen, M. A. Second Harmonic Generation Microscopy Reveals

https://doi.org/10.1021/jacs.0c10777
J. Am. Chem. Soc. XXXX, XXX, XXX−XXX

Hidden Polar Organization in Fluoride Doped MIL-53(Fe). *Dalton Trans.* **2016**, *45*, 4401−4406.
(180) Simenas, M.; Balciunas, S.; Trzebiatowska, M.; Ptak, M.; Maczka, M.; Volkel, G.; Poppl, A.; Banys, J. Electron Paramagnetic Resonance and Electric Characterization of a $CH_3NH_2NH_2Zn(HCOO)_3$ Perovskite Metal Formate Framework. *J. Mater. Chem. C* **2017**, *5*, 4526−4536.
(181) Zhang, W.; Xiong, R. G. Ferroelectric Metal-Organic Frameworks. *Chem. Rev.* **2012**, *112*, 1163−1195.
(182) Krause, S.; Evans, J. D.; Bon, V.; Senkovska, I.; Ehrling, S.; Iacomi, P.; Tobbens, D. M.; Wallacher, D.; Weiss, M. S.; Zheng, B.; Yot, P. G.; Maurin, G.; Llewellyn, P. L.; Coudert, F. X.; Kaskel, S. Engineering Micromechanics of Soft Porous Crystals for Negative Gas Adsorption. *Chem. Sci.* **2020**, *11*, 9468−9479.
(183) Schaber, J.; Krause, S.; Paasch, S.; Senkovska, I.; Bon, V.; Tobbens, D. M.; Wallacher, D.; Kaskel, S.; Brunner, E. in Situ Monitoring of Unique Switching Transitions in the Pressure Amplifying Flexible Framework Material DUT-49 by High-Pressure Xe-129 NMR Spectroscopy. *J. Phys. Chem. C* **2017**, *121*, 5195−5200.

https://doi.org/10.1021/jacs.0c10777
J. Am. Chem. Soc. XXXX, XXX, XXX−XXX